SCIENCE CHINA Information Sciences



RESEARCH PAPER

 $\begin{array}{c} {\rm January~2026,~Vol.~69,~Iss.~1,~112302:1-112302:19} \\ {\rm ~https://doi.org/10.1007/s11432-024-4325-5} \end{array}$

Enhancing radar stealth performance through radar network resource allocation for multi-target tracking: a counter-sorting approach

Lei ZHANG¹, Dan WANG^{1*}, Huan WANG², Jianfei REN¹ & Ying LUO¹

¹Institute of Information and Navigation, Air Force Engineering University, Xi'an 710077, China ²Xi'an Electronic Engineering Research Institute, Xi'an 710077, China

Received 10 July 2024/Revised 3 December 2024/Accepted 1 March 2025/Published online 22 September 2025

Abstract The electronic interception system requires capturing a sufficiently long and relevant pulse traffic to determine the presence of a radiation source. This paper originates from active countermeasures perspectives and introduces a multi-radar resource allocation scheme in multi-target tracking scenarios to counteract pulse deinterleaving. Our study aims to enhance radar network stealth while preserving tracking accuracy by leveraging the collaborative capabilities of networked radars. We establish and analyze the signal model of multiple co-located multiple input multiple output radars tracking multiple targets and find that radar-controllable variables such as radiation power, duty cycle, and dwell time can impact both tracking precision and interceptable pulse length by interception receivers. Unlike conventional radar radio frequency stealth methods focused solely on single-pulse detection, we optimize these variables to reduce both probabilities of individual pulse interception and pulse traffic deinterleaving or sorting, lowering overall radar interception risks. Simulation results confirm the efficacy of our methodology in bolstering radar network resilience against reconnaissance threats while maintaining robust target detection capabilities. This research underscores the importance of optimizing radar resource management strategies to achieve a balanced trade-off between detection performance and stealth capability in practical deployment scenarios.

Keywords radar network, multi-radar resource allocation, multi-target tracking, radio frequency stealth, probability of interception, pulse deinterleaving

Citation Zhang L, Wang D, Wang H, et al. Enhancing radar stealth performance through radar network resource allocation for multi-target tracking: a counter-sorting approach. Sci China Inf Sci, 2026, 69(1): 112302, https://doi.org/10.1007/s11432-024-4325-5

1 Introduction

Radar electronic counter-countermeasures (ECCM) work to mitigate the effects of electronic countermeasure (ECM) on radar performance, ensure radar detection, identification, and tracking of targets effectively [1–4], and can be categorized into active and passive countermeasures according to the purpose of use. Passive countermeasures like sidelobe cancellation [5], sidelobe blanking [6], subspace projection [7], and blind source separation [8] perform to identify and filter out jamming signals after being interfered with and thus may lose some helpful signal while filtering out the interference. Active anti-jamming technology aims to increase the difficulty of jamming devices carrying out jamming and, therefore, has received widespread attention.

From the perspective of radar ECM, the process involves intercepting radar signals, detecting the radiation source based on parameters measurement and pulse deinterleaving, assessing the threat level of the radiation source, and then making jamming decisions [9]. Thus, employing low probability of intercept (LPI) techniques to enhance the difficulty of intercepting radar signals and subsequent radar emitters is the onset of active countermeasures [10]. About the quantification of radio frequency (RF) stealth performance, multiple quantitative metrics have been proposed in [11–13], among which, the intercept probability model based on window functions has gained widespread application for simple and precise. This model views the interception of radar signals as a probability issue of overlaps in multiple domains, such as space, time, frequency, and energy, that is, calculating the probability of radar signals falling into various reconnaissance windows of the intercept receiver and being detectable. Therefore, controlling radiation to alter the distribution of radar signals across different domains can reduce the probability of interception. For instance, controlling radar radiated power is the most direct way to achieve radar LPI [14]. In addition, controlling the spatial distribution of radar signal energy through beamforming techniques can lower

^{*} Corresponding author (email: wangdan0709@126.com)

the probability of detection from sidelobes [15, 16]. Frequency diverse array radars can also manage the energy distribution across the range dimension, becoming another implementation of LPI radars [17, 18]. Additionally, controlling energy distribution in the time domain, such as adjusting the radar revisit intervals and dwell times [19], can similarly alter the radar's LPI performance. Apart from these, optimizing the radar waveform is also an effective way to achieve radar LPI detection [20,21]. However, limited by finite detection resources, it is challenging for a single radar to balance detection performance with stealth capabilities.

The radar network system is one system that links multiple spatially separated radars to achieve collaborative detection and information fusion on targets [22–25]. Compared with single-radar systems, radar networks possess richer detection resources, which can be flexibly configured under unified control to maximize the detection efficiency of the system. Leveraging such superiority, numerous scholars have investigated LPI technologies for radar networks, aiming to minimize the radiation risk while fulfilling detection tasks. For instance, sensor scheduling issues for singletarget tracking, that is, selecting the optimal sensor at each tracking time to minimize cumulative radiation risk is explored in [26, 27] and for multi-target tracking scenarios, that is, allocating tracking radars to each target to balance tracking accuracy and stealth performance is studied in [28–32]. When the number of radars and targets is large, this radar-target assignment problem becomes computationally intensive, leading [33] to propose an efficient solution based on machine learning. These sensor scheduling-based approaches for radar networks are explored when the radar emission modes are fixed. When radiation parameters of the networked radars, like radiation power and revisit intervals, are controllable, numerous scholars optimize them to lower the interception probability of the radar network in different application scenarios [34,35]. Additionally, integrating radiation control with sensor scheduling to achieve RF stealth for radar networks is also studied in [36-40], and which has extended controllable resources to more aspects such as flight paths of node radars (in mobile radar networks like airborne radar networks), radiation power, dwell time, waveform bandwidth, and pulse length, further enhancing the flexibility of resource allocation within the radar network.

The basic principle of electronic reconnaissance equipment intercepting radiation sources relies on the consistent emission of radar signal sources during operation. If the regularity of this emission pattern can be found from the intercepted pulse traffic, the presence of the radiation source can be determined. The intercepted pulse from a specified radiation source must not only fall within the reconnaissance window and be detectable but also avoid losing it due to the simultaneous arrival of multiple pulses. Although there has been considerable research on radar resource allocation strategies under LPI guidance, much of this research has primarily focused on pulse interception, with less emphasis on subsequent pulse sorting and emitter interception. Therefore, to enhance the LPI performance of radar systems, efforts should be directed toward reducing the length of pulse flow intercepted by the intercept receiver by not only reducing the probability of pulse signal interception but also increasing the probability of pulse loss and finalizing the goal of decreasing the probability of pulse sorting, which is what we do in this manuscript.

This paper proposes a resource control and beam allocation scheme for multi-radar cooperative tracking of multiple targets under the guidance of against pulse deinterleaving. First, the signal model of multi-radar cooperative tracking of multiple targets is established, and the mathematical expression of the posterior Cramér-Rao lower bound (PCRLB) [41] is derived. Then, the radar radiation parameters that jointly affect the tracking accuracy and stealth performance are determined. Based upon this foundation, an optimization model with radiation power, duty cycle, dwell time, and beam allocation as variables constrained by target tracking precision to enhance the stealth performance of the radar network is established, and an alternating minimization method is employed to solve this model.

The innovativeness of this paper is mainly reflected in the following three points.

- We establish a signal processing model for multi-target tracking in a co-located multiple input multiple output (MIMO) radar network. Each radar emits wide beams covering the entire surveillance area and receives signals from different targets through multiple narrow beams. Each radar locally estimates angle and Doppler parameters using maximum likelihood estimation from observation data, followed by data fusion and global estimation using extended Kalman filter (EKF) [42] in the information fusion center to minimize information loss.
- We develop a resource allocation model for radar network systems with LPI capabilities, combining antiintercept for a single pulse with anti-sorting for pulse traffic. Existing RF stealth solutions often focus solely on low-pulse-interception performance. Building upon this foundation, we consider subsequent pulse sorting processes to enhance RF stealth performance. Our approach involves reducing dwell time to decrease pulse train length and optimizing the duty cycle to increase pulse loss, thereby further reducing the sorting probability of the radar pulses.
- We employ pulse sorting probability to characterize the LPI performance of the radar network. Existing literature predominantly focuses on LPI-oriented resource optimization, with limited intuitive descriptions of LPI performance enhancement. In simulation experiments, we use multi-radar pulse sorting probability to characterize the stealth performance of the radar network.

This article is structured as follows. Section 2 presents the signal model of the radar network. Section 3 introduces the target tracking process. Section 4 derives the mathematical expression of PCRLB. Section 5 formulates resource allocation as an optimization problem and solves it. Section 6 confirms the performance of the proposed resource optimization scheme through numerical examples. Lastly, we conclude this paper in Section 7.

Notation. In this paper, vectors are defined in lowercase bold, and matrices in uppercase bold. $(\cdot)^{\mathrm{T}}$, $(\cdot)^{\dagger}$, and $(\cdot)^{-1}$ denote transpose, conjugate transpose, and inverse, respectively. The symbol \otimes denotes the Kronecker product. $x \sim \mathcal{CN}(m, \Sigma)$ denotes that x obeys a Gaussian distribution with m as the mean and Σ as the covariance. $\mathbb{E}\{\cdot\}$ means the mathematical expectation. $\mathbb{R}^{N\times M}$ denotes the set of $(N\times M)$ -dimensional real and matrices. $\Re(\cdot)$ represents the extraction of the real part. $[\cdot]_{i,j}$ stands for the i-th row j-th column element of a matrix, and $[\cdot]_i$ stands for the i-th element of a vector.

2 Signal model

Consider a radar network system comprising N time-synchronized radars that monitor Q moving targets. Each radar node is the co-located MIMO radar operated in a "defocused transmit-focused receive" mode [43], where the transmitter emits orthogonal signals from each array element to form wide beams covering the entire surveillance area. Digital beamforming techniques are employed at the receiver to form multiple narrow beams to track different targets.

2.1 Target motion model

Assuming Q targets undergo linear constant-velocity motion in the XOY plane, and the motion state of the q-th target at frame k is defined as $\mathbf{x}_k^q = [x_k^q, \dot{x}_k^q, y_k^q, \dot{y}_k^q]^T$. Thus, the motion state of the q-th target can be expressed as

$$x_k^q = F x_{k-1}^q + u_{k-1}^q. (1)$$

Here, F serves as the target state transition matrix, expressed as

$$\boldsymbol{F} = \boldsymbol{I}_2 \otimes \begin{bmatrix} 1 & \Delta T \\ 0 & 1 \end{bmatrix}, \tag{2}$$

and ΔT is the revisit interval. u_{k-1}^q is the zero-mean Gaussian process noise with covariance matrix Q_q defined as

$$Q_q = \kappa_q \mathbf{I}_2 \otimes \begin{bmatrix} (\Delta T)^3 / 3 \ (\Delta T)^2 / 2 \\ (\Delta T)^2 / 2 \ \Delta T \end{bmatrix}, \tag{3}$$

where κ_q is the noise intensity during state transition.

2.2 Radar measurement model

Take the *n*-th radar node as an example. Assume it is located at $[x_n, y_n]$ with M_{tn} transmit array elements and M_{rn} receive array elements. At the *k*-th frame, it emits $L_{k,n}$ pulses with pulse width T_{dn} to trace the target. The relationship between $L_{k,n}$ and the dwell time $T_{dwk,n}$ is $T_{dwk,n} = L_{k,n}T_{rk,n}$, where $T_{rk,n}$ represents the pulse repetition interval (PRI) of radar *n* at frame *k*. Let $\boldsymbol{\mu}_{k,n} = [\mu_{k,n}^1, \dots, \mu_{k,n}^Q]^T$ denote the radar-target assignment between radar *n* and the *Q* targets at frame *k*. $\mu_{k,n}^q \in \{0,1\}$ indicates whether radar *n* measures target *q* at frame *k*, with $\mu_{k,n}^q = 1$ indicating measurement on target *q*, and $\mu_{k,n}^q = 0$ indicating no measurement. If $\mu_{k,n}^q = 1$, the $l_{k,n}$ -th pulse received by radar *n* regarding target *q* at frame *k* can be expressed as

$$\mathbf{s}_{k,n}^{q,l_{k,n}}(t) = \sqrt{\alpha_{k,n}^q P_{tk,n} / M_{tn} h_{k,n}^q \boldsymbol{\alpha}_{rn} \left(\theta_{k,n}^q\right) \boldsymbol{\alpha}_{tn}^T \left(\theta_{k,n}^q\right) \boldsymbol{s}_n \left(t - \tau_{k,n}^q\right)} \cdot \exp\left\{-j2\pi f_{dk,n}^q \left(l_{k,n} - 1\right) T_{rk,n}\right\}.$$

$$(4)$$

Here, $\alpha_{k,n}^q \propto 1/(R_{k,n}^q)^4$ denotes the propagation loss, $R_{k,n}^q$ is the distance between target q and radar n, $P_{tk,n}$ represents the peak power of radar n at frame k, $h_{k,n}^q$, $\theta_{k,n}^q$, $\tau_{k,n}^q$, and $f_{dk,n}^q$, respectively, stands for the radar cross section (RCS), the azimuth angle, the propagation delay, and the Doppler frequency of target q relative to radar n

at frame k. $s_n(t) = [s_{n,1}(t), \dots, s_{n,M_{tn}}(t)]^T$ represents the transmission signal vector of radar n, where the signals are orthogonal to each other, satisfying

$$\int_0^{T_{\rm dn}} \boldsymbol{s}_n(t) \boldsymbol{s}_n^{\dagger}(t) \mathrm{d}t = \boldsymbol{I}_{M_{\rm tn}}.$$
 (5)

 $\alpha_{\mathrm{r}n}$ and $\alpha_{\mathrm{t}n}$ are the receive and transmit steering vector of radar n, respectively, satisfying

$$\boldsymbol{\alpha}_{\mathrm{r}n}\left(\boldsymbol{\theta}_{k,n}^{q}\right) = \begin{bmatrix} 1 & \mathrm{e}^{-\mathrm{j}\phi_{\mathrm{r}k,n}^{q}} & \cdots & \mathrm{e}^{-\mathrm{j}(M_{\mathrm{r}n}-1)\phi_{\mathrm{r}k,n}^{q}} \end{bmatrix}^{\mathrm{T}}$$
(6)

and

$$\boldsymbol{\alpha}_{\mathrm{t}n}\left(\boldsymbol{\theta}_{k,n}^{q}\right) = \begin{bmatrix} 1 & \mathrm{e}^{-\mathrm{j}\phi_{\mathrm{t}k,n}^{q}} & \cdots & \mathrm{e}^{-\mathrm{j}(M_{\mathrm{t}n}-1)\phi_{\mathrm{t}k,n}^{q}} \end{bmatrix}^{\mathrm{T}}$$
(7)

with $\phi_{\mathrm{r}k,n}^q = 2\pi d_{\mathrm{r}n} \sin \theta_{k,n}^q / \lambda_n$ and $\phi_{\mathrm{t}k,n}^q = 2\pi d_{\mathrm{t}n} \sin \theta_{k,n}^q / \lambda_n$. $d_{\mathrm{r}n}$ and $d_{\mathrm{t}n}$ represent the interval between receive elements and transmit elements of radar n, respectively. λ_n stands for the wavelength of radar n. It is noted that Eq. (4) neglects intra-pulse Doppler.

Upon receiving the signal, radar n performs matched filtering with $s_{n,m}(t-\tau_{k,n}^q)$, $m=1,\ldots,M_{tn}$ to obtain an observation vector of dimension $M_{tn}M_{rn}\times 1$, expressed as

$$\boldsymbol{z}_{k,n}^{q,l_{k,n}} = \xi_{k,n}^{q} \exp\left\{-j2\pi f_{\mathrm{d}k,n}^{q} \left(l_{k,n} - 1\right) T_{\mathrm{r}k,n}\right\} \left(\boldsymbol{\alpha}_{\mathrm{t}n} \left(\boldsymbol{\theta}_{k,n}^{q}\right) \otimes \boldsymbol{\alpha}_{\mathrm{r}n} \left(\boldsymbol{\theta}_{k,n}^{q}\right)\right),\tag{8}$$

where $\xi_{k,n}^q = \sqrt{\alpha_{k,n}^q P_{\mathrm{t}k,n}/M_{\mathrm{t}n}} h_{k,n}^q$. The same process is applied to $L_{k,n}$ pulses, and then $\{z_{k,n}^{q,l_{k,n}}\}_{l_{k,n}=1}^{L_{k,n}}$ are stacked into an observation vector of dimension $L_{k,n} M_{\mathrm{t}n} M_{\mathrm{r}n} \times 1$, which can be written as

$$\boldsymbol{z}_{k,n}^{q} = \left[\left(\boldsymbol{z}_{k,n}^{q,1} \right)^{\mathrm{T}}, \dots, \left(\boldsymbol{z}_{k,n}^{q,L_{k,n}} \right)^{\mathrm{T}} \right]^{\mathrm{T}}$$

$$= \xi_{k,n}^{q} \boldsymbol{\alpha}_{\mathrm{d}n} \left(f_{\mathrm{d}k,n}^{q} \right) \otimes \left(\boldsymbol{\alpha}_{\mathrm{t}n} \left(\theta_{k,n}^{q} \right) \otimes \boldsymbol{\alpha}_{\mathrm{r}n} \left(\theta_{k,n}^{q} \right) \right), \tag{9}$$

where $\alpha_{dn}(f_{dk,n}^q)$ denotes the Doppler steering vector of target q relative to radar n at frame k, defined as

$$\boldsymbol{\alpha}_{\mathrm{d}n}\left(f_{\mathrm{d}k,n}^{q}\right) = \begin{bmatrix} 1 & \mathrm{e}^{-\mathrm{j}\phi_{\mathrm{d}k,n}^{q}} & \cdots & \mathrm{e}^{-\mathrm{j}(L_{k,n}-1)\phi_{\mathrm{d}k,n}^{q}} \end{bmatrix}^{\mathrm{T}}$$
(10)

with $\phi_{\mathrm{d}k,n}^q = 2\pi f_{\mathrm{d}k,n}^q T_{\mathrm{r}k,n}$. If the presence of additive Gaussian noise is considered in observation duration, the covariance matrix of which is assumed to be $C_n = \sigma_n^2 I_{L_{k,n} M_{\mathrm{t}n} M_{\mathrm{r}n}}$ with σ_n^2 the noise intensity, we have

$$\boldsymbol{z}_{k,n}^{q} \sim \mathcal{N}\left(\boldsymbol{\mu}_{k,n}^{q}, \boldsymbol{C}_{n}\right),$$
 (11)

where $\boldsymbol{\mu}_{k,n}^q = \xi_{k,n}^q \boldsymbol{\alpha}_{\mathrm{d}n}(f_{\mathrm{d}k,n}^q) \otimes (\boldsymbol{\alpha}_{\mathrm{t}n}(\theta_{k,n}^q) \otimes \boldsymbol{\alpha}_{\mathrm{r}n}(\theta_{k,n}^q))$. As inferred from (9), both $\theta_{k,n}^q$ and $f_{\mathrm{d}k,n}^q$ can be directly estimated from the observation vector $\boldsymbol{z}_{k,n}^q$. Let $\boldsymbol{\zeta}_{k,n}^q = [\theta_{k,n}^q, f_{\mathrm{d}k,n}^q]^{\mathrm{T}}$, and then the maximum likelihood estimation of $\boldsymbol{\zeta}_{k,n}^q$, denoted as $\hat{\boldsymbol{\zeta}}_{k,n}^q$, can be obtained from the following equations:

$$\left\{ \hat{\boldsymbol{\zeta}}_{k,n}^{q}, \hat{\boldsymbol{\xi}}_{k,n}^{q} \right\} = \underset{\boldsymbol{\zeta}_{k,n}^{q}, \boldsymbol{\xi}_{k,n}^{q}}{\operatorname{arg\,max}} \ln p \left(\boldsymbol{z}_{k,n}^{q} | \boldsymbol{\zeta}_{k,n}^{q}, \boldsymbol{\xi}_{k,n}^{q} \right) \\
= \underset{\boldsymbol{\zeta}_{k,n}^{q}, \boldsymbol{\xi}_{k,n}^{q}}{\operatorname{arg\,min}} \frac{1}{\sigma_{n}^{2}} \left\| \boldsymbol{z}_{k,n}^{q} - \boldsymbol{\mu}_{k,n}^{q} \right\|^{2}.$$
(12)

Since the target states \boldsymbol{x}_k^q and $\boldsymbol{\zeta}_{k,n}^q$ can be related by the following nonlinear equation:

$$\zeta_{k,n}^{q} = g_{n} \left(\boldsymbol{x}_{k}^{q} \right) = \begin{bmatrix} \arctan\left(\frac{y_{k}^{q} - y_{n}}{x_{k}^{q} - x_{n}}\right) \\ -\frac{2\left(\dot{x}_{k}^{q} \left(x_{k}^{q} - x_{n}\right) + \dot{y}_{k}^{q} \left(y_{k}^{q} - y_{n}\right)\right)}{\lambda_{n} \sqrt{\left(x_{k}^{q} - x_{n}\right)^{2} + \left(y_{k}^{q} - y_{n}\right)^{2}}} \end{bmatrix},$$
(13)

the measurement model of radar n on target q can be expressed as

$$\hat{\zeta}_{k,n}^{q} \sim \mathcal{N}\left(g_{n}\left(\boldsymbol{x}_{k}^{q}\right), \boldsymbol{R}_{k,n}^{q}\right),\tag{14}$$

where $\mathbf{R}_{k,n}^q$ is the estimation error covariance matrix, which can be approximated to the Cramér-Rao lower bound (CRLB) matrix under high SNR conditions.

3 Target tracking process

For target q, let $\varpi_k^q = \{n | \mu_{k,n}^q = 1\}$ be the set of radars tracking it at frame k. When target q is tracked by multiple radars simultaneously, i.e., $|\varpi_k^q| > 1$, information fusion is required. Here $|\varpi_k^q|$ represents the cardinality of the set ϖ_k^q . Each radar directly sends local measurements to the central fusion center for global fusion to enhance tracking accuracy and reduce information loss. The global measurement $\hat{\zeta}_k^q$ of target q is constructed by concatenating local measurements $\hat{\zeta}_{k,n}^q$ from the radars involved in tracking the target at that frame, and can be written as

$$\hat{\zeta}_{k}^{q} = \left[\hat{\zeta}_{k,\varpi_{k}^{q}(1)}^{q T}, \hat{\zeta}_{k,\varpi_{k}^{q}(2)}^{q T}, \dots, \hat{\zeta}_{k,\varpi_{k}^{q}(|\varpi_{k}^{q}|)}^{q T}\right]^{T}, \tag{15}$$

where $\varpi_k^q(n)$ denotes the *n*-th element of the set ϖ_k^q . Correspondingly, the global measurement model for target q can be expressed as

$$\hat{\zeta}_{k}^{q} \sim \mathcal{N}\left(g\left(\boldsymbol{x}_{k}^{q}\right), \boldsymbol{R}_{k}^{q}\right),\tag{16}$$

where

$$g\left(\boldsymbol{x}_{k}^{q}\right) = \left[g_{\varpi_{k}^{q}\left(1\right)}^{\mathrm{T}}\left(\boldsymbol{x}_{k}^{q}\right), g_{\varpi_{k}^{q}\left(2\right)}^{\mathrm{T}}\left(\boldsymbol{x}_{k}^{q}\right), \dots, g_{\varpi_{k}^{q}\left(\left|\varpi_{k}^{q}\right|\right)}^{\mathrm{T}}\left(\boldsymbol{x}_{k}^{q}\right)\right]^{\mathrm{T}},\tag{17}$$

and

$$\boldsymbol{R}_{k}^{q} = \text{blkdiag}\left\{\boldsymbol{R}_{k,\varpi_{k}^{q}(1)}^{q}, \boldsymbol{R}_{k,\varpi_{k}^{q}(2)}^{q}, \dots, \boldsymbol{R}_{k,\varpi_{k}^{q}(|\varpi_{k}^{q}|)}^{q}\right\}.$$
(18)

For the nonlinear measurement models illustrated in (16) and (17), nonlinear filters can be employed to estimate the target state. EKF is an extension of the Kalman filter, which handles nonlinear systems by employing Taylor series expansions in the state transition and measurement models. Compared with particle filter [44], EKF based on analytical solutions typically has lower computational complexity. Considering the conservation of computational resources, this paper opts for EKF to estimate the target state. The estimates of the target state \hat{x}_k^q and its covariance matrix Σ_k^q at each frame can be sequentially calculated as follows:

$$\hat{\boldsymbol{x}}_{k|k-1}^q = \boldsymbol{F}\hat{\boldsymbol{x}}_{k-1}^q,\tag{19a}$$

$$\Sigma_{k|k-1}^q = Q_q + F \Sigma_{k-1}^q F^{\mathrm{T}}, \tag{19b}$$

$$\hat{\boldsymbol{x}}_{k}^{q} = \hat{\boldsymbol{x}}_{k|k-1}^{q} + \boldsymbol{K}_{k}^{q} \left(\hat{\boldsymbol{\zeta}}_{k}^{q} - g \left(\hat{\boldsymbol{x}}_{k|k-1}^{q} \right) \right), \tag{19c}$$

$$\Sigma_k^q = \Sigma_{k|k-1}^q - K_k^q G_k^q \Sigma_{k|k-1}^q, \tag{19d}$$

where K_k^q is the Kalman gain, calculated by

$$K_{k}^{q} = \Sigma_{k|k-1}^{q} G_{k}^{q \, \mathrm{T}} \left(G_{k}^{q} \Sigma_{k|k-1}^{q} G_{k}^{q \, \mathrm{T}} + R_{k}^{q} \right)^{-1}. \tag{20}$$

Note that $G_k^q \in \mathbb{N}^{2|\varpi_k^q| \times 4}$ is the Jacobian matrix of the function $g(\boldsymbol{x}_k^q)$ with respect to \boldsymbol{x}_k^q , defined as

$$\boldsymbol{G}_{k}^{q} = \begin{bmatrix} \boldsymbol{G}_{k,\varpi_{k}^{q}(1)}^{q} \\ \boldsymbol{G}_{k,\varpi_{k}^{q}(2)}^{q} \\ \vdots \\ \boldsymbol{G}_{k,\varpi_{k}^{q}(|\varpi_{k}^{q}|)}^{q} \end{bmatrix}, \tag{21}$$

and $G_{k,n}^q \in \mathbb{N}^{2\times 4}$ is the Jacobian matrix of the function $g_n(\boldsymbol{x}_k^q)$ with respect to \boldsymbol{x}_k^q , defined as

$$\boldsymbol{G}_{k,n}^{q} = \begin{bmatrix} \partial \theta_{k,n}^{q} / \partial x_{k}^{q} & \partial \theta_{k,n}^{q} / \partial \dot{x}_{k}^{q} & \partial \theta_{k,n}^{q} / \partial y_{k}^{q} & \partial \theta_{k,n}^{q} / \partial \dot{y}_{k}^{q} \\ \partial f_{\mathrm{d}k,n}^{q} / \partial x_{k}^{q} & \partial f_{\mathrm{d}k,n}^{q} / \partial \dot{x}_{k}^{q} & \partial f_{\mathrm{d}k,n}^{q} / \partial y_{k}^{q} & \partial f_{\mathrm{d}k,n}^{q} / \partial \dot{y}_{k}^{q} \end{bmatrix}.$$
 (22)

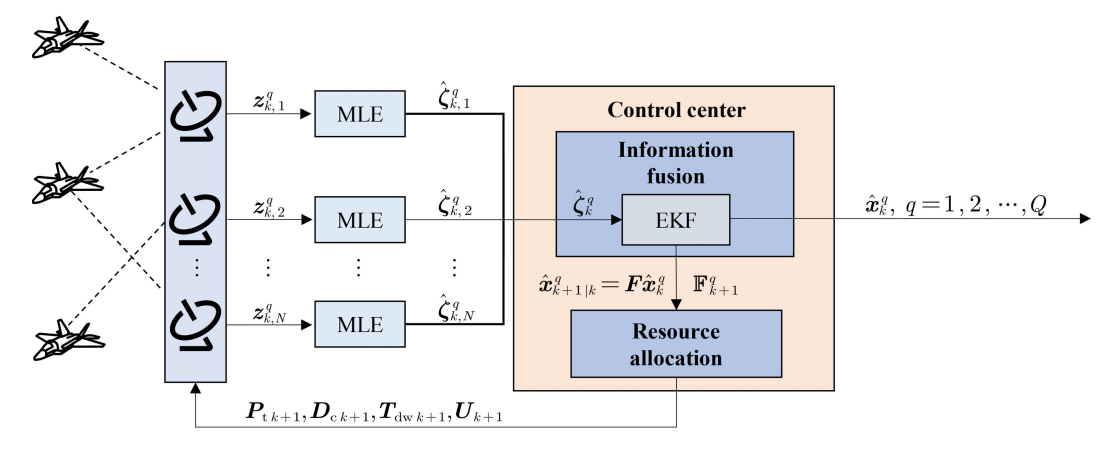


Figure 1 Closed-loop tracking procedure.

The elements in the first row are

$$\frac{\partial \theta_{k,n}^{q}}{\partial x_{k}^{q}} = \frac{y_{n} - y_{k}^{q}}{\left(x_{k}^{q} - x_{n}\right)^{2} + \left(y_{k}^{q} - y_{n}\right)^{2}},\tag{23a}$$

$$\frac{\partial \theta_{k,n}^q}{\partial y_k^q} = \frac{x_k^q - x_n}{(x_k^q - x_n)^2 + (y_k^q - y_n)^2},$$
(23b)

$$\frac{\partial \theta_{k,n}^q}{\partial \dot{x}_k^q} = \frac{\partial \theta_{k,n}^q}{\partial \dot{y}_k^q} = 0, \tag{23c}$$

and in the second row are

$$\frac{\partial f_{dk,n}^q}{\partial x_k^q} = -\frac{2(y_k^q - y_n)(\dot{x}_k^q (y_k^q - y_n) - \dot{y}_k^q (x_k^q - x_n))}{\lambda_n \left((x_k^q - x_n)^2 + (y_k^q - y_n)^2 \right)^{3/2}},$$
(24a)

$$\frac{\partial f_{dk,n}^q}{\partial y_k^q} = -\frac{2(x_k^q - x_n)(\dot{y}_k^q (x_k^q - x_n) - \dot{x}_k^q (y_k^q - y_n))}{\lambda_n \left((x_k^q - x_n)^2 + (y_k^q - y_n)^2 \right)^{3/2}},$$

$$\frac{\partial f_{dk,n}^q}{\partial \dot{x}_k^q} = -\frac{2(x_k^q - x_n)}{\lambda_n \sqrt{(x_k^q - x_n)^2 + (y_k^q - y_n)^2}},$$
(24b)

$$\frac{\partial f_{dk,n}^{q}}{\partial \dot{x}_{k}^{q}} = -\frac{2(x_{k}^{q} - x_{n})}{\lambda_{n} \sqrt{(x_{k}^{q} - x_{n})^{2} + (y_{k}^{q} - y_{n})^{2}}},$$
(24c)

$$\frac{\partial f_{dk,n}^{q}}{\partial \dot{y}_{k}^{q}} = -\frac{2(y_{k}^{q} - y_{n})}{\lambda_{n} \sqrt{(x_{k}^{q} - x_{n})^{2} + (y_{k}^{q} - y_{n})^{2}}}.$$
(24d)

Figure 1 depicts the closed-loop tracking framework of the proposed radar network in a multi-target scenario. The target tracking accuracy \mathbb{F}_k^q and the resource allocation strategy will be described in Sections 4 and 5, respectively.

4 Target tracking accuracy characterization

To ensure the effectiveness of radar detection, we must analyze the relationship between radiation parameters and radar performance (target tracking accuracy in tracking scenarios). Therefore, it is imperative first to establish a mathematical model that quantitatively characterizes target tracking accuracy. PCRLB describes the lower bound for parameter estimation accuracy given prior information and observed data and, therefore, is commonly used as a performance metric in dynamic parameter estimation problems such as target tracking. The definition of PCRLB matrix C_{PCRLB} is [41]

$$\mathbb{E}_{\boldsymbol{x}_{k}^{q},\boldsymbol{z}_{k}^{q}}\left\{\left(\hat{\boldsymbol{x}}_{k}^{q}\left(\boldsymbol{z}_{k}^{q}\right)-\boldsymbol{x}_{k}^{q}\right)\left(\hat{\boldsymbol{x}}_{k}^{q}\left(\boldsymbol{z}_{k}^{q}\right)-\boldsymbol{x}_{k}^{q}\right)^{\mathrm{T}}\right\} \succeq \boldsymbol{J}^{-1}\left(\boldsymbol{x}_{k}^{q}\right) \triangleq \boldsymbol{C}_{\mathrm{PCRLB}}\left(\boldsymbol{x}_{k}^{q}\right). \tag{25}$$

Here, $\boldsymbol{z}_k^q = \{\boldsymbol{z}_{k,n}^q | n \in \varpi_k^q\}$ represents all observation for target q at frame k, and $\boldsymbol{J}(\boldsymbol{x}_k^q)$ is the Fisher information matrix (FIM), computed as

$$\boldsymbol{J}\left(\boldsymbol{x}_{k}^{q}\right) = -\mathbb{E}_{\boldsymbol{x}_{k}^{q},\boldsymbol{z}_{k}^{q}}\left\{\Delta_{\boldsymbol{x}_{k}^{q}}^{\boldsymbol{x}_{k}^{q}} \ln p\left(\boldsymbol{x}_{k}^{q},\boldsymbol{z}_{k}^{q}\right)\right\},\tag{26}$$

where $\Delta_{\psi}^{\theta} = \nabla_{\psi} \nabla_{\theta}^{T}$, and ∇_{θ} means the first-order partial derivative of the vector θ . Since $p(\boldsymbol{x}_{k}^{q}, \boldsymbol{z}_{k}^{q})$ can be written as

$$p\left(\boldsymbol{x}_{k}^{q}, \boldsymbol{z}_{k}^{q}\right) = p\left(\boldsymbol{x}_{k}^{q}\right) p\left(\boldsymbol{z}_{k}^{q} \middle| \boldsymbol{x}_{k}^{q}\right), \tag{27}$$

 $J(x_k^q)$ can also be further written as

$$J\left(\boldsymbol{x}_{k}^{q}\right) = J_{\mathrm{p}}\left(\boldsymbol{x}_{k}^{q}\right) + J_{\mathrm{D}}\left(\boldsymbol{x}_{k}^{q}\right),\tag{28}$$

where

$$\boldsymbol{J}_{P}\left(\boldsymbol{x}_{k}^{q}\right) = -\mathbb{E}_{\boldsymbol{x}_{k}^{q}}\left\{\Delta_{\boldsymbol{x}_{k}^{q}}^{\boldsymbol{x}_{k}^{q}}\ln p\left(\boldsymbol{x}_{k}^{q}\right)\right\},\tag{29a}$$

$$\boldsymbol{J}_{\mathrm{D}}\left(\boldsymbol{x}_{k}^{q}\right) = -\mathbb{E}_{\boldsymbol{x}_{k}^{q},\boldsymbol{z}_{k}^{q}}\left\{\Delta_{\boldsymbol{x}_{k}^{q}}^{\boldsymbol{x}_{k}^{q}}\ln p\left(\boldsymbol{z}_{k}^{q}|\boldsymbol{x}_{k}^{q}\right)\right\},\tag{29b}$$

and they represent the parts of the FIM from prior knowledge and observed data, respectively. According to [41] and the linear motion model depicted in (1), $J_{\rm P}(x_k^q)$ can be recursively computed as

$$J_{P}\left(\boldsymbol{x}_{k}^{q}\right) = \boldsymbol{D}_{k-1}^{q,22} - \boldsymbol{D}_{k-1}^{q,21} \left(J\left(\boldsymbol{x}_{k-1}^{q}\right) + \boldsymbol{D}_{k-1}^{q,11}\right)^{-1} \boldsymbol{D}_{k-1}^{q,12},\tag{30}$$

where

$$\begin{cases}
D_{k-1}^{q,11} = -\mathbb{E}_{\boldsymbol{x}_{k-1}^q, \boldsymbol{x}_k^q} \left\{ \Delta_{\boldsymbol{x}_{k-1}^q}^{\boldsymbol{x}_{k-1}^q} \ln p\left(\boldsymbol{x}_k^q | \boldsymbol{x}_{k-1}^q\right) \right\} = \boldsymbol{F}^{\mathrm{T}} \boldsymbol{Q}_q^{-1} \boldsymbol{F}, \\
D_{k-1}^{q,12} = -\mathbb{E}_{\boldsymbol{x}_{k-1}^q, \boldsymbol{x}_k^q} \left\{ \Delta_{\boldsymbol{x}_k^q}^{\boldsymbol{x}_{k-1}} \ln p\left(\boldsymbol{x}_k^q | \boldsymbol{x}_{k-1}^q\right) \right\} = -\boldsymbol{F}^{\mathrm{T}} \boldsymbol{Q}_q^{-1} = \left(\boldsymbol{D}_{k-1}^{q,21}\right)^{\mathrm{T}}, \\
D_{k-1}^{q,22} = -\mathbb{E}_{\boldsymbol{x}_{k-1}^q, \boldsymbol{x}_k^q} \left\{ \Delta_{\boldsymbol{x}_k^q}^{\boldsymbol{x}_k} \ln p\left(\boldsymbol{x}_k^q | \boldsymbol{x}_{k-1}^q\right) \right\} = \boldsymbol{Q}_q^{-1}.
\end{cases} (31)$$

Therefore, $J_{\rm P}(x_k^q)$ can be expressed as

$$J_{P}\left(\boldsymbol{x}_{k}^{q}\right) = \left[\boldsymbol{Q}_{q} + \boldsymbol{F}\boldsymbol{J}^{-1}\left(\boldsymbol{x}_{k-1}^{q}\right)\boldsymbol{F}^{T}\right]^{-1}.$$
(32)

For $J_D(x_k^q)$, when the observations of target q by each radar are mutually independent, we have

$$J_{D}(\boldsymbol{x}_{k}^{q}) = -\mathbb{E}_{\boldsymbol{x}_{k}^{q}} \left\{ \mathbb{E}_{\boldsymbol{z}_{k}^{q} | \boldsymbol{x}_{k}^{q}} \left\{ \Delta_{\boldsymbol{x}_{k}^{q}}^{\boldsymbol{x}_{k}^{q}} \ln p\left(\boldsymbol{z}_{k}^{q} | \boldsymbol{x}_{k}^{q}\right) \right\} \right\}$$

$$= \sum_{n \in \varpi_{k}^{q}} \mathbb{E}_{\boldsymbol{x}_{k}^{q}} \left\{ -\mathbb{E}_{\boldsymbol{z}_{k,n}^{q} | \boldsymbol{x}_{k}^{q}} \left\{ \Delta_{\boldsymbol{x}_{k}^{q}}^{\boldsymbol{x}_{k}^{q}} \ln p\left(\boldsymbol{z}_{k,n}^{q} | \boldsymbol{x}_{k}^{q}\right) \right\} \right\}$$

$$\triangleq \sum_{n \in \varpi_{k}^{q}} \mathbb{E}_{\boldsymbol{x}_{k}^{q}} \left\{ J_{D}^{n}(\boldsymbol{x}_{k}^{q}) \right\}. \tag{33}$$

Since \boldsymbol{z}_k^q is directly associated with $\boldsymbol{\zeta}_{k,n}^q$ rather than \boldsymbol{x}_k^q , applying the chain rule can transform $\boldsymbol{J}_{\mathrm{D}}^n(\boldsymbol{x}_k^q)$ into

$$J_{\mathrm{D}}^{n}(\boldsymbol{x}_{k}^{q}) = \boldsymbol{G}_{k,n}^{q \mathrm{T}} J_{\mathrm{D}}^{n} \left(\boldsymbol{\zeta}_{k,n}^{q}\right) \boldsymbol{G}_{k,n}^{q}, \tag{34}$$

where $G_{k,n}^q$ can be calculated with (22), and $J_{\mathrm{D}}^n(\zeta_{k,n}^q)$ is expressed as

$$J_{\mathcal{D}}^{n}\left(\zeta_{k,n}^{q}\right) = -\mathbb{E}_{\boldsymbol{z}_{k,n}^{q}|\zeta_{k,n}^{q}}\left\{\Delta_{\zeta_{k,n}^{q}}^{\zeta_{k,n}^{q}} \ln p\left(\boldsymbol{z}_{k,n}^{q}|\zeta_{k,n}^{q}\right)\right\}. \tag{35}$$

After some algebraic calculations, the approximate expression of $J_{\mathcal{D}}^n(\zeta_{k,n}^q)$ can be given by

$$J_{\mathrm{D}}^{n}\left(\zeta_{k,n}^{q}\right) \approx P_{\mathrm{t}k,n} D_{\mathrm{c}k,n} J_{n}\left(\zeta_{k,n}^{q}, T_{\mathrm{dw}k,n}\right),\tag{36}$$

where $D_{ck,n} = T_{dn}/T_{rk,n}$ is the duty cycle of radar n at frame k, and $J_n(\zeta_{k,n}^q, T_{dwk,n})$ is defined as

$$J_{n}(\zeta_{k,n}^{q}, T_{\text{dw}k,n}) \triangleq \begin{bmatrix} T_{\text{dw}k,n} A_{k,n}^{q} & T_{\text{dw}k,n}^{2} C_{k,n}^{q} \\ T_{\text{dw}n}^{2} C_{k,n}^{q} & T_{\text{dw}k,n}^{3} B_{k,n}^{q} \end{bmatrix}.$$
(37)

The derivative process and the expression of $A_{k,n}^q$, $B_{k,n}^q$, and $C_{k,n}^q$ can be seen in Appendix A.

According to (33), computing $J_{\rm D}(x_k^q)$ entails calculating the mathematical expectation, which can be achieved through Monte Carlo methods. However, to meet the real-time requirements of target tracking and reflect the proactive nature of resource allocation, the zero-process noise prediction $\hat{x}_{k|k-1}^q = F\hat{x}_{k-1}^q$ can be substituted for x_k^q . Summing up the above, $J(x_k^q)$ can be defined as

$$J(x_{k}^{q}) = \left[Q_{q} + FJ^{-1}\left(x_{k-1}^{q}\right)F^{T}\right]^{-1} + \sum_{n=1}^{N} \mu_{k,n}^{q} P_{tk,n} D_{ck,n} G_{k,n}^{q T} J_{n}\left(\zeta_{k,n}^{q}, T_{dwk,n}\right) G_{k,n}^{q} \Big|_{\hat{x}_{k|k-1}^{q}}.$$
 (38)

5 Problem formulation and solving

Simultaneous operation under unified control of multiple radars not only reduces the radiated power of each radar but also creates a complex pulse stream that increases the difficulty of sorting by the intercepting receiver, further reducing the probability of the radar being intercepted.

5.1 Two assumptions

Assumption 1. Electronic intercept receiver passively intercepts non-cooperative radar signals. Due to cost, size, power constraints, and the need to address unknown sources and the response time requirements, electronic intercept receivers resort to single-channel wide-open receivers to capture all types of radar signals across frequency, spatial, and temporal domains. Thus, the first assumption is that radar pulse signals will inevitably fall within the reconnaissance window of the intercept receiver. At this point, only the detection probability for individual pulses needs to be considered [45,46]:

$$P_{\rm d} = \frac{1}{2} \operatorname{erfc} \left(\sqrt{-\ln P_{\rm fa}} - \sqrt{\operatorname{SNR}_{\rm I} + 0.5} \right), \tag{39}$$

where

$$\operatorname{erfc}(z) = 1 - \frac{2}{\pi} \int_0^z e^{-v^2} dv.$$
 (40)

Here SNR_I represents the output SNR of a single pulse at the intercept receiver, expressed as

$$SNR_{I} = \frac{P_{t}G_{t}G_{r}G_{p}\lambda_{t}^{2}F_{p}^{2}}{(4\pi)^{2}R^{2}L_{p}k_{B}T_{0}BN_{F}},$$
(41)

where $P_{\rm t}$ denotes the radar radiated power, $G_{\rm t}$, $G_{\rm r}$, and $G_{\rm p}$ represent the transmit gain of the radar in the direction of the intercept receiver, the receive gain of the intercept receiver in the direction of the radar, and the processing gain of the intercept receiver, respectively, $\lambda_{\rm t}$ stands for the wavelength, $F_{\rm p}$ signifies the propagation factor, R indicates the distance from the radar to the intercept receiver, $L_{\rm p}$ accounts for polarization loss, $k_{\rm B}$ represents the Boltzmann constant, with a value of 1.38×10^{-23} J/K, $T_{\rm 0}$ denotes the noise temperature, B stands for the bandwidth of the intercept receiver, and $N_{\rm F}$ signifies the noise figure of the intercept receiver. It can be observed that reducing the radar radiated power can decrease the probability of radar pulses being detected by the intercept receiver.

Assumption 2. When multiple radiation sources are simultaneously operational, the electronic intercept equipment receives multiple interleaved pulse streams, leading to a high likelihood of pulse loss. For instance, if the arrival time of two pulses is less than the width of the first pulse, these two pulses will overlap, resulting in deviations in parameter measurements and causing pulse loss. The specific pulse loss or the loss of both pulses depends on the degree of overlap and the amplitude difference between the two pulses. Furthermore, for an instantaneous frequency measurement receiver, there exists a recovery period after completing the parameter measurement of one pulse, during which newly arriving pulses are not processed and thus discarded. To quantitatively describe the

probability of pulse loss, we simplify the model by making the second assumption that one pulse will be lost when it enters the intercept receiver while the previous pulse is still being processed, and the processing duration is equal to the pulse width. Therefore, the capture process of pulses by the wide-open intercept equipment can be described using the single-server loss system model from queueing theory [47], and the probability of pulse loss P_1 can be approximated as

$$P_{\rm l} = \frac{\lambda_{\rm p} \tau_{\rm p}}{1 + \lambda_{\rm p} \tau_{\rm p}},\tag{42}$$

where $\lambda_{\rm p}$ denotes the pulse density and $\tau_{\rm p}$ signifies the average processing duration of a single pulse. In the scenario of multiple radars emitting simultaneously, $\lambda_{\rm p}\tau_{\rm p}$ can also be regarded as the total duty cycle of the pulse traffic. As seen, a higher duty cycle results in higher pulse loss; therefore, it is possible to increase the probability of pulse loss by adjusting each radar's duty cycle and increasing the pulse traffic's total duty cycle.

5.2 Problem formulation

From (38), it is evident that \mathbb{F}_k^q is related to P_{tk} , D_{ck} , T_{dwk} , and U_k . From (39), it is understood that the probability of a radar signal being detected by the intercept receiver is associated with the respective radar radiated powers $P_{tk,n}$. According to (42), the probability of pulse loss is dependent on the total duty cycle of the pulse traffic $\sum_{n=1}^{N} D_{ck,n}$. Furthermore, the total number of pulses emitted by each radar at each frame is related to the dwell time $T_{dwk,n}$, duty cycle $D_{ck,n}$, and pulse width T_{dn} of each radar, as $L_{k,n} = T_{dwk,n}D_{ck,n}/T_{dn}$. Therefore, to achieve active countermeasures, the radar network system should strategically optimize the radiation parameters like $P_{tk,n}$, $D_{ck,n}$, and $T_{dwk,n}$ of each radar at every tracking frame, along with their assignment with targets, to reduce the length of the pulse traffic intercepted by the intercept receiver and ultimately reduce the probability of sorting the radiation source from it.

Let $P_{tk} = [P_{tk,1}, \dots, P_{tk,N}]^T$, $D_{ck} = [D_{ck,1}, \dots, D_{ck,N}]^T$, and $T_{dwk} = [T_{dwk,1}, \dots, T_{dwk,N}]^T$ denote the radiated power, duty cycle, and dwell time vector for the radar network at frame k, respectively, and $U_k = [\mu_{k,1}, \dots, \mu_{k,N}]$ represent the radar-target assignment matrix. The objective function of the aforementioned resource optimization problem can be formulated as

$$\mathbb{F}(\mathbf{P}_{tk}, \mathbf{D}_{ck}, \mathbf{T}_{dwk}, \mathbf{U}_k) = \sum_{n=1}^{N} \frac{T_{dwk,n} D_{ck,n}}{T_{dn}} + \alpha_1 \sum_{n=1}^{N} P_{tk,n} - \alpha_2 \sum_{n=1}^{N} D_{ck,n},$$
(43)

where α_1 and α_2 are weighting coefficients. In the above objective function, the first term is intended to control the length of the burst emitted by each radar, the second term is intended to control the probability of interception of each radar pulse, and the third term is intended to control the probability of pulse loss for the entire pulse traffic. In addition, let

$$\mathbb{F}_{k}^{q} = \sqrt{\operatorname{Tr}\left[C_{\text{PCRLB}}\left(\boldsymbol{x}_{k}^{q}\right)\right]}$$
(44)

denote the measure of target tracking accuracy. The aforementioned resource optimization problem can be expressed as

$$\min_{\mathbf{P}_{tk}, \mathbf{D}_{ck}, T_{dwk}, U_{k}} \mathbb{F}\left(\mathbf{P}_{tk}, \mathbf{D}_{ck}, T_{dwk}, U_{k}\right),$$

$$\begin{cases}
\mathbb{F}_{k}^{q} \leqslant \mathbb{F}_{\max}^{q}, \forall q = 1, \dots, Q, \\
P_{tn}^{\min} \leqslant P_{tk,n} \leqslant P_{tn}^{\max}, \forall n = 1, \dots, N, \\
D_{cn}^{\min} \leqslant D_{ck,n} \leqslant D_{cn}^{\max}, \forall n = 1, \dots, N, \\
T_{dwn}^{\min} \leqslant T_{dwk,n} \leqslant T_{dwn}^{\max}, \forall n = 1, \dots, N,
\end{cases}$$
s.t.
$$\begin{cases}
Q \\
\sum_{q=1}^{q} \mu_{k,n}^{q} \leqslant \mu_{n}, \forall n = 1, \dots, N, \\
1 \leqslant \sum_{n=1}^{N} \mu_{k,n}^{q} \leqslant N, \forall q = 1, \dots, Q,
\end{cases}$$

$$(45)$$

where the constraint $\mathbb{F}_k^q \leqslant \mathbb{F}_{\max}^q$ ensures that the tracking error of each target does not exceed the upper bound \mathbb{F}_{\max}^q ; $P_{\text{tn}}^{\min} \leqslant P_{\text{tk},n} \leqslant P_{\text{tn}}^{\max}$, $D_{\text{cn}}^{\min} \leqslant D_{\text{ck},n} \leqslant D_{\text{cn}}^{\max}$, and $T_{\text{dwn}}^{\min} \leqslant T_{\text{dwk},n} \leqslant T_{\text{dwn}}^{\max}$ respectively constrain the radiation power, duty cycle, and dwell time of each radar within certain intervals; $\sum_{q=1}^Q \mu_{k,n}^q = \mu_n$ indicates that each radar can simultaneously form up to μ_n receive beams; $1 \leqslant \sum_{n=1}^N \mu_{k,n}^q \leqslant N$ requires that each target is tracked by at least one radar. By reducing the number of radiated pulses per radar and increasing pulse loss (by controlling the radiated power to reduce the probability of detection and managing the total duty cycle to increase the pulse overlap), it is possible to reduce the length of the pulse traffic intercepted by the intercepting receiver and increase the difficulty of pulse sorting.

5.3 Model solution

Due to the existence of the 0-1 variables $\mu_{k,n}^q$, the aforementioned problem constitutes a non-convex, non-linear mixed-integer programming problem. One exhaustive search approach involves enumerating all possible assignment relationships between radar beams and targets based on the constraints $\sum_{q=1}^Q \mu_{k,n}^q \leqslant \mu_n$ and $1 \leqslant \sum_{n=1}^N \mu_{k,n}^q \leqslant N$, and then optimizing P_{tk} , D_{ck} , and T_{dwk} to minimize the objective function. At this point, the problem can be reformulated as

$$\min_{\mathbf{U}_{k}} \left\{ \min_{\mathbf{P}_{tk}, \mathbf{D}_{ck}, \mathbf{T}_{\text{dw}k}} \mathbb{F}\left(\mathbf{P}_{tk}, \mathbf{D}_{ck}, \mathbf{T}_{\text{dw}k}; \mathbf{U}_{k}\right) \right\},$$
s.t.
$$\begin{cases}
\mathbb{F}_{k}^{q} \leqslant \mathbb{F}_{\text{max}}^{q}, \forall q = 1, \dots, Q, \\
P_{tn}^{\text{min}} \leqslant P_{tk, n} \leqslant P_{tn}^{\text{max}}, \forall n = 1, \dots, N, \\
D_{cn}^{\text{min}} \leqslant D_{ck, n} \leqslant D_{cn}^{\text{max}}, \forall n = 1, \dots, N, \\
T_{\text{dwn}}^{\text{min}} \leqslant T_{\text{dw}k, n} \leqslant T_{\text{dwn}}^{\text{max}}, \forall n = 1, \dots, N.
\end{cases} (46)$$

Given U_k , for such a constrained nonlinear programming problem, the interior-point method is employed for a solution.

However, this exhaustive search approach is time-consuming and unsuitable for real-time processing. Therefore, relaxing $\mu_{k,n}^q$ to continuous values within the interval [0, 1] should be considered. Since U_k is actually independent of the objective function $\mathbb{F}(P_{tk}, D_{ck}, T_{dwk}, U_k)$ but only influences tracking accuracy \mathbb{F}_k^q , U_k and other variables can be alternatingly solved. Specifically, initializing P_{tk} , D_{ck} , and T_{dwk} , solving for U_k can follow the model below:

$$\min_{\mathbf{U}_{k}} \quad \sum_{q=1}^{Q} \mathbb{F}_{k}^{q},$$
s.t.
$$\begin{cases}
\sum_{q=1}^{Q} \mu_{k,n}^{q} = \mu_{n}, \forall n = 1, \dots, N, \\
1 \leqslant \sum_{n=1}^{N} \mu_{k,n}^{q} \leqslant N, \forall q = 1, \dots, Q.
\end{cases}$$
(47)

That is, given P_{tk} , D_{ck} , and T_{dwk} , optimizing U_k to minimize the tracking error of each target as much as possible. This optimization problem is solved using the interior-point method. Assuming the obtained relaxed solution is U_{k0} , a feasible solution U_k conforming to the original problem needs to be constructed. The specific approach is as follows: setting U_k to be a zero matrix, first arranging each column of U_{k0} in ascending order and finding the position of the maximum value, assigning 1 to that position in U_k to ensure each target is tracked; second, arranging each row of the matrix U_{k0} in ascending order, selecting the largest μ_n elements (subtracting the count of elements already selected or too small like below 0.1), assigning 1 to the corresponding positions in U_k to ensure that each radar's receive beams are tracking targets. Once the feasible solution U_k is obtained, solving the following optimization problem yields feasible solutions for P_{tk} , D_{ck} , T_{dwk} :

$$\min_{\mathbf{P}_{tk}, \mathbf{D}_{ck}, \mathbf{T}_{dwk}} \mathbb{F}\left(\mathbf{P}_{tk}, \mathbf{D}_{ck}, \mathbf{T}_{dwk}; \mathbf{U}_{k}\right),$$
s.t.
$$\begin{cases}
\mathbb{F}_{k}^{q} \leqslant \mathbb{F}_{\max}^{q}, \forall q = 1, \dots, Q, \\
P_{tn}^{\min} \leqslant P_{tk,n} \leqslant P_{tn}^{\max}, \forall n = 1, \dots, N, \\
D_{cn}^{\min} \leqslant D_{ck,n} \leqslant D_{cn}^{\max}, \forall n = 1, \dots, N, \\
T_{dwn}^{\min} \leqslant T_{dwk,n} \leqslant T_{dwn}^{\max}, \forall n = 1, \dots, N.
\end{cases} \tag{48}$$

Table 1 Simulation parameters for targets.

Target	Position (km)	Velocity (m/s)	RCS (m ²)	
1	[11, 17]	[-78, -31]	4	
2	[20, 24]	[10, 38]	4	
3	[7, 12]	[-57, -87]	2	
4	[19, 10]	[-70, 8]	4	

Table 2 Simulation parameters for radars.

Radar	Position (km)	$P_{\rm t}$ (W)	D _c (%)	$T_{\rm dw}~({\rm ms})$	$T_{\rm d}~(\mu { m s})$	μ
1	[0, 15]	[1477, 7341]	[1.7, 9]	[48, 260]	19	3
2	[0, 30]	[1641, 7267]	[0.8, 14]	[35, 390]	20	3
3	[15, 30]	[1056, 7934]	[1.2, 13]	[20, 290]	16	3
4	[30, 15]	[1126, 4754]	[1.7, 5]	[24, 130]	11	3
5	[30, 0]	[1151, 7007]	[0.6, 6]	[36, 440]	12	3
6	[15, 0]	[1348, 4059]	[0.6, 18]	[39, 390]	20	2

This alternating process continues until the absolute difference between the objective function values $\mathbb{F}(P_{tk}, D_{ck}, T_{dwk}; U_k)$ of two consecutive iterations is less than a predetermined threshold. Then, the final P_{tk} , D_{ck} , T_{dwk} , and U_k are output.

6 Simulation results

This section is devoted to designing simulation experiments to validate the effectiveness of the proposed resource optimization and beam allocation scheme in reducing the probability of intercepting radiation sources by the intercept receiver.

6.1 Simulation parameters

Assuming 6 co-ocated MIMO radars are monitoring 4 moving targets on a two-dimensional plane. The simulation parameters like initial position and velocity for each target are provided in Table 1. The position and other simulation parameters of each radar are listed in Table 2, where the transmit power, duty cycle, and dwell time are controllable variables distributed within certain ranges, while pulse width and the number of simultaneous beams are invariant parameters. The radar revisit interval $\Delta T = 1$ s, and the tracking process lasts for 50 frames. Other parameters are set as $\lambda_n = 0.3$ m, $\kappa_q = 10^{-4}$, and $\sigma_n = 1$.

There are two points to be clarified. One is that the preset upper bound of tracking error is not always constant but decreases linearly with the tracking process to realize the gradual improvement of the tracking accuracy, and the initial values are 65, 175, 105, and 85 m, respectively; and the second is that the initial FIM of all the targets is replaced by Q_q , i.e., $\mathbb{F}_0^q = \sqrt{\text{Tr}[Q_q^{-1}]} = 566$ m for all the targets.

6.2 Tracking validation

Figure 2 illustrates the radar distribution and target trajectories during the tracking process. The dashed lines in Figure 2 represent the target trajectories estimated from one Monte Carlo test, while the solid line represents the actual trajectories. It can be observed that the proposed resource allocation scheme ensures real-time and accurate target tracking by the networked radars.

Figure 3 presents the optimized radiated power, duty cycle, and dwell time during the tracking process. Note that these values have been normalized. Taking the radiated power as an example, assume that the optimization yields a power of $\hat{P}_{\mathrm{tk},n}$, which after normalization becomes

$$\bar{P}_{tk,n} = \frac{\hat{P}_{tk,n} - P_{tn}^{\min}}{P_{tn}^{\max} - P_{tn}^{\min}}.$$
(49)

Therefore, when the value of $\bar{P}_{tk,n}$ is 1, it indicates maximum power radiation and a value of 0 indicates minimum power radiation.

As seen, when the targets move, their distances from each radar vary, necessitating dynamic adjustments to the emission parameters of radars to maintain tracking accuracy. In particular, the values of all radiation parameters are

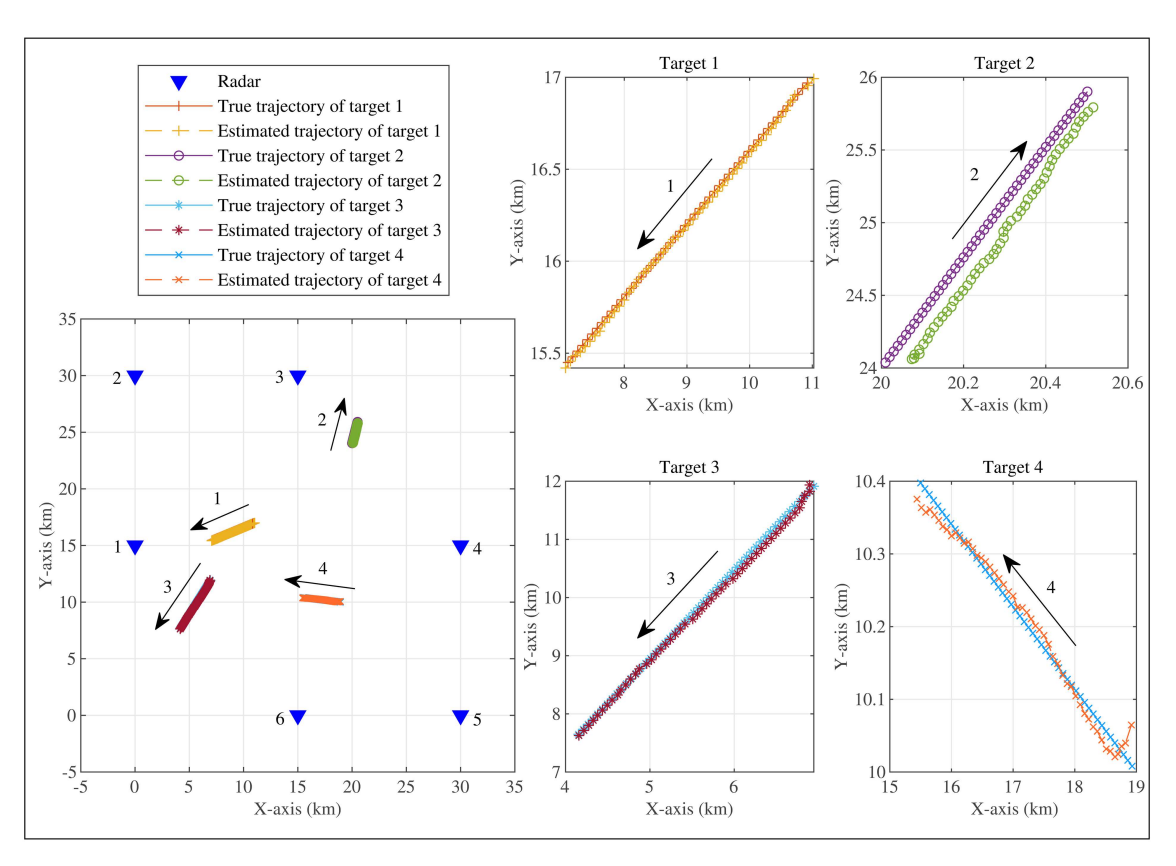


Figure 2 Scene diagram. The left figure shows the radar distribution, target tracks, and estimated trajectories. The 4 figures on the right are zoomed-in views of each target's trajectory.

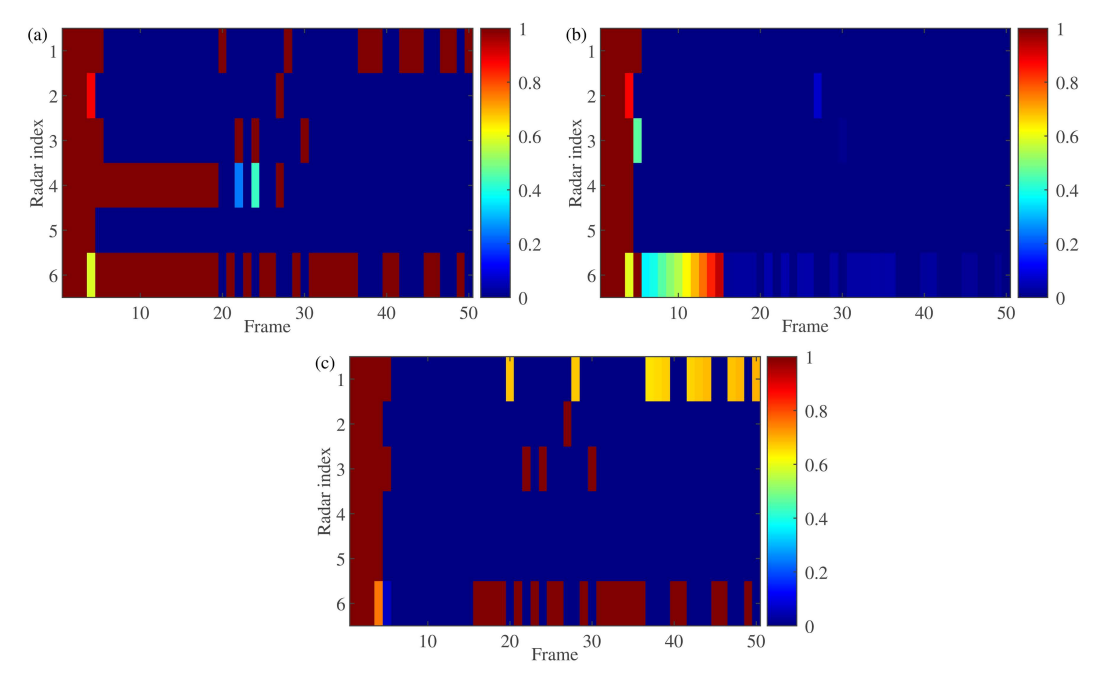


Figure 3 Variation of the radar radiation parameters. (a) Radiated power; (b) duty cycle; (c) dwell time.

significant at the beginning of the tracking (first five frames) and become small from the sixth frame onwards, and the variation trend of radiated power overlaps with dwell time to a greater extent. This is because the system needs to increase the radiated power and the number of pulses to enhance the tracking accuracy due to the significant tracking error at the beginning of the tracking phase, while the LPI requirement makes the duty cycle of each radar

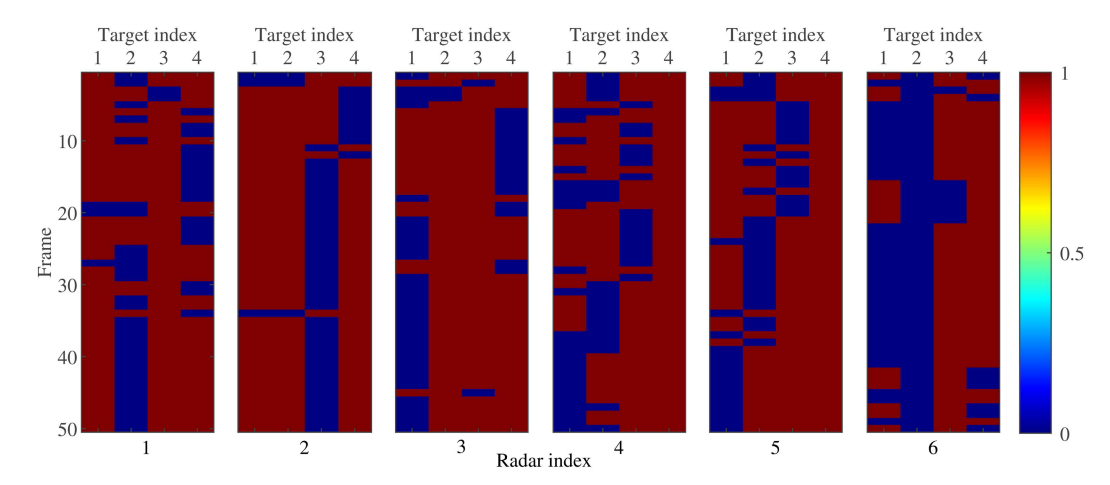


Figure 4 Beam distribution scheme of each radar.

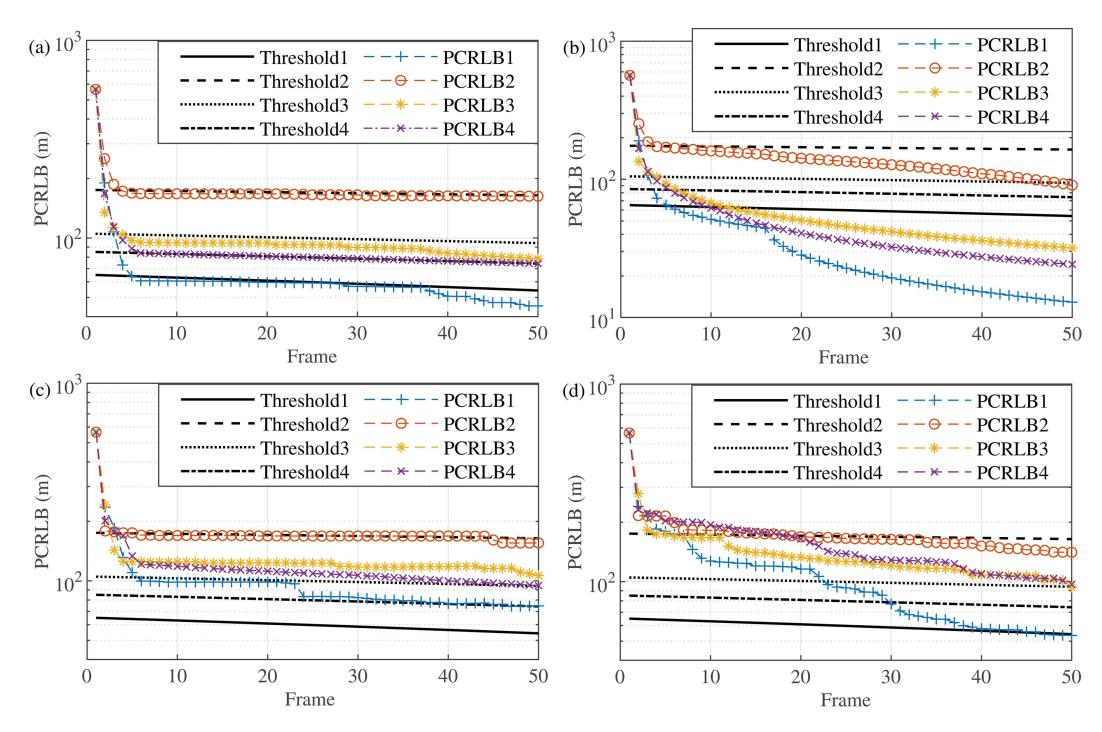


Figure 5 PCRLB obtained by different resource allocation schemes. Here, let threshold+i denote the preset tracking accuracy requirement for the i-th target and PCRLB+i denote the PCRLB of the i-th target. (a) CM; (b) MTEM; (c) MIPM; (d) RM.

increase to increase the pulse loss and shorten the length of the pulse string intercepted by the interceptor receiver. When the system enters the stable tracking phase, the LPI requirement reduces the radiated power and the number of pulses significantly, thus eliminating the need for excessive modulation of the duty cycle to increase pulse loss, so the value of the duty cycle becomes small after the sixth frame. Regarding the value of radiated power and dwell time of the sixth radar, which is always large, one possible explanation is that radar 6 has a smaller number of simultaneously trackable targets and contributes less to tracking the entire target population, thus requiring an increase in radiated power and dwell time.

Figure 4 illustrates the beam allocation throughout the process. It is evident that each radar dynamically adjusts its selection of tracked objects rather than fixedly tracking specific targets. Moreover, most of the time, each radar assigns all available beams to targets while only a few times tracks the target less than the available beams.

To quantitatively describe the tracking accuracy under the proposed resource allocation scheme, Figure 5 depicts the \mathbb{F}_k^q curves for each target. For comparison purposes, Figure 5 also separately illustrates the impact of three other resource allocation schemes on target tracking accuracy. The first comparative strategy is the minimum tracking error mode (MTEM), which disregards the stealth performance of the radar network system and only optimizes resource allocation to minimize tracking errors at each frame. The solving process of MTEM is similar to the alter-

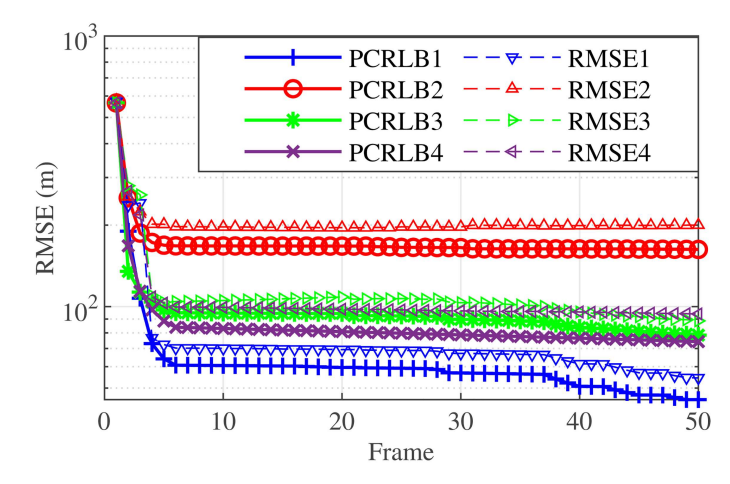


Figure 6 Variation of the RMSE of each target. Here, let RMSE+i denote the RMSE of the *i*-th target.

nating minimization method used in this paper but transforms the objective function into min $\sum_{q=1}^{Q} \mathbb{F}_{k}^{q}$. The second comparative strategy is the minimum interception probability mode (MIPM), which disregards tracking errors at each frame, optimizing resource allocation to reduce the interception probability of the radar network system. The optimization variables P_{tk} , D_{ck} , and T_{dwk} are solved in a manner similar to (48), while the beam allocation matrix U_k is randomly generated subject to meeting $\sum_{q=1}^{Q} \mu_{k,n}^q \leq \mu_n, \forall n=1,\ldots,N$. The third comparative method is the random power + random duty cycle + random dwell time mode, where the beam allocation matrix U_k is also randomly generated, referred to as the random mode (RM). All three comparative methods assume radars randomly track targets up to the beam bound. This section calls our resource allocation strategy a comprehensive mode (CM), i.e., balancing tracking accuracy and stealth performance. In the MTEM and our CM, the tracking error consistently remains below the preset threshold, meeting the radar network system's accuracy requirements for multi-target tracking. In contrast, in the MIPM and RM, the tracking accuracy of the remaining targets fails to meet the task requirements except for the second target.

The \mathbb{F}_k^q used in Figure 5 represents the computed or predicted tracking accuracy. Therefore, the root mean square error (RMSE) for each target, namely RMSE, is adopted to characterize the actual tracking accuracy, which is defined as

$$RMSE_{k}^{q} = \sqrt{\frac{1}{N_{MC}} \sum_{n=1}^{N_{MC}} \|\hat{\boldsymbol{x}}_{k,n}^{q} - \boldsymbol{x}_{k}^{q}\|_{F}^{2}},$$
(50)

where $\hat{\boldsymbol{x}}_{k,n}^q$ denotes the estimated target state obtained from the *n*-th Monte Carlo test, while \boldsymbol{x}_k^q represents the true target state. From Figure 6, it can be observed that, over time, RMSE_k^q gradually converges to the PCRLB. Note here $N_{\text{MC}} = 1000$.

6.3 Low intercept verification

This subsection verifies the low interception of the networked radar under the proposed resource allocation scheme in this paper through simulation experiments. We measure the radar network's resistance to interception by assessing the ease of deinterleaving pulse sequences emitted by each radar from the pulse traffic. The technique of pulse deinterleaving based on pulse repetition interval (PRI) information is widely used, and in this section, we employ the PRI transformation method [48] to perform pulse deinterleaving. The PRI transformation method involves converting the differences in arrival times of a pulse sequence into the PRI spectrum through a complex-valued autocorrelation integral transformation. The position of the peak on the spectrum's horizontal axis corresponds to the estimated PRI value of the pulse sequence. In other words, if the PRI transformation value at a certain point on the PRI spectrum exceeds the detection threshold, the corresponding horizontal axis coordinate is considered the PRI estimate. For quantitative comparison, we assume the existence of intercept receivers at the center of the scene, namely at [15,15] km. Under the resource allocation scheme proposed in this paper, the low interception of the radar network will manifest in three aspects: First, each radar emits short bursts by controlling dwell time and duty cycle. Second, reducing radiated power decreases the probability of individual pulses being detected. Assuming at frame k, the interception receiver can intercept the maximum power pulse with $P_{\rm fa} = 10^{-4}$ and $P_{\rm d} = 0.999$. Here,

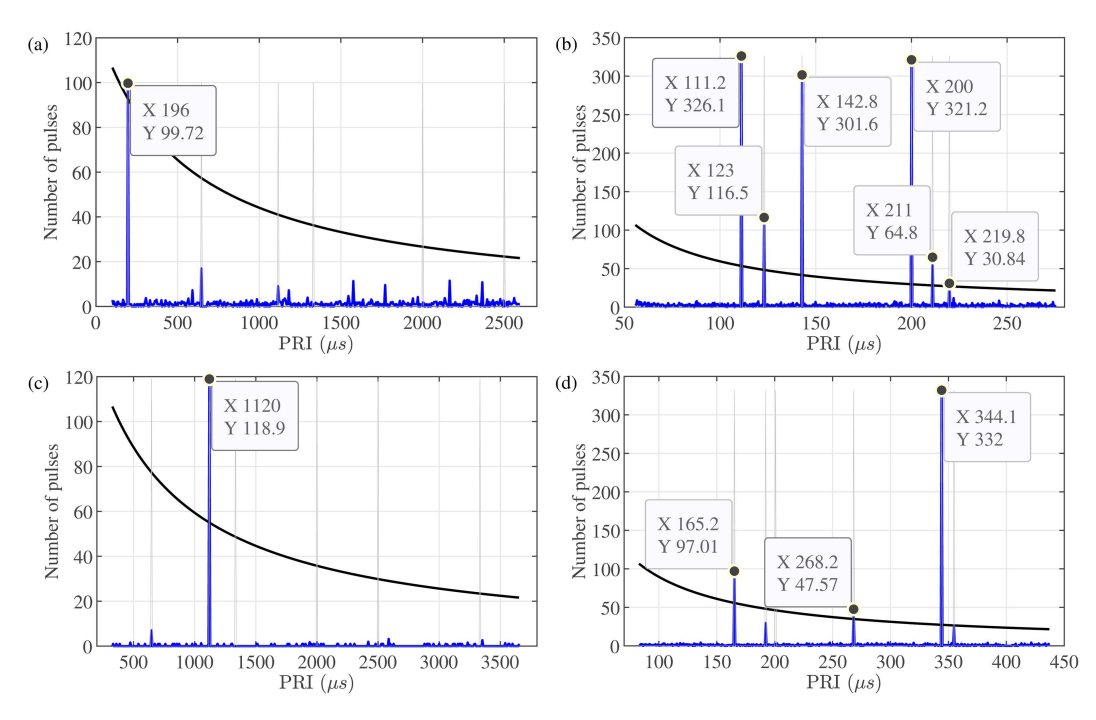


Figure 7 PRI spectra at frame 10 for four resource allocation strategies. The black solid line indicates the detection threshold, and the gray vertical line indicates the location of the true PRI. (a) CM; (b) MTEM; (c) MIPM; (d) RM.

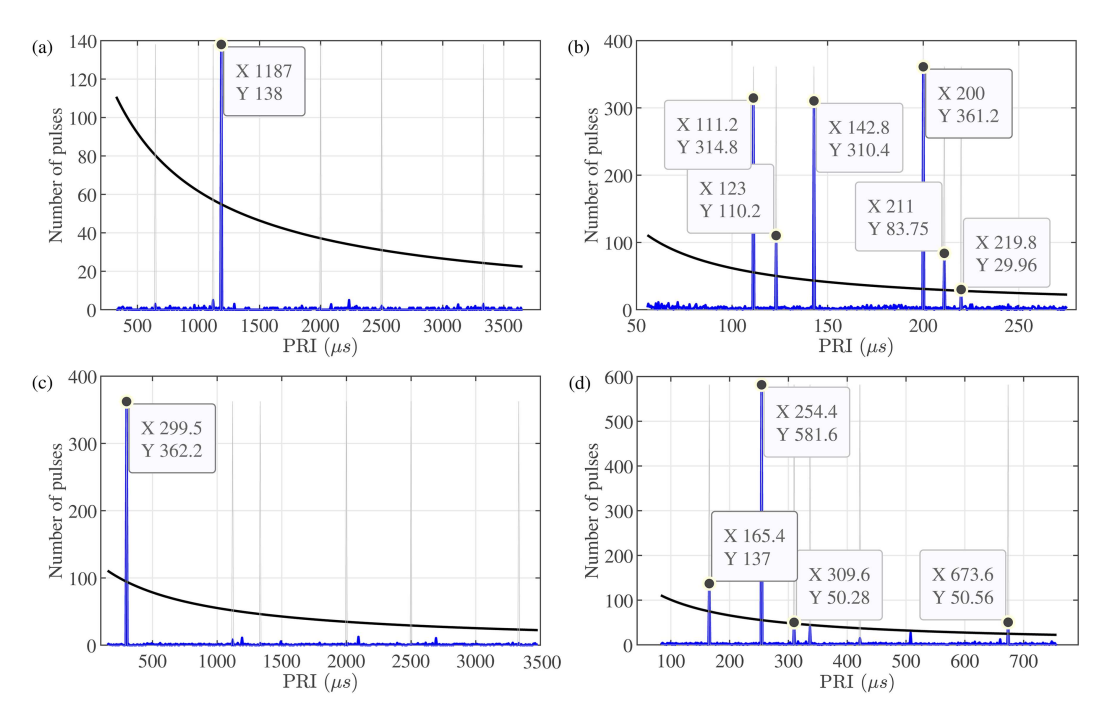


Figure 8 PRI spectra at frame 30 for four resource allocation strategies. (a) CM; (b) MTEM; (c) MIPM; (d) RM.

the maximum power refers to the maximum of $P_{tk,n}/R_{In}$, where R_{In} is the distance between the interception device and radar n. Assume all other parameters are the same. By applying (39) and (41), the detection probability for pulses of each radar can be calculated, and these pulses are selectively intercepted according to this probability. Here, interception refers to detection. Third, pulse overlap leads to an increase in lost pulses. As analyzed earlier, pulse loss occurs when the interval between the arrival times of the two pulse fronts is less than the width of the first pulse. In this simulation, we assume that the second pulse is lost. As the total duty cycle of the pulse traffic increases, the number of lost pulses due to overlap also increases.

Figures 7 and 8 depict the PRI spectra for the four resource allocation schemes at the 10-th and 30-th frames,

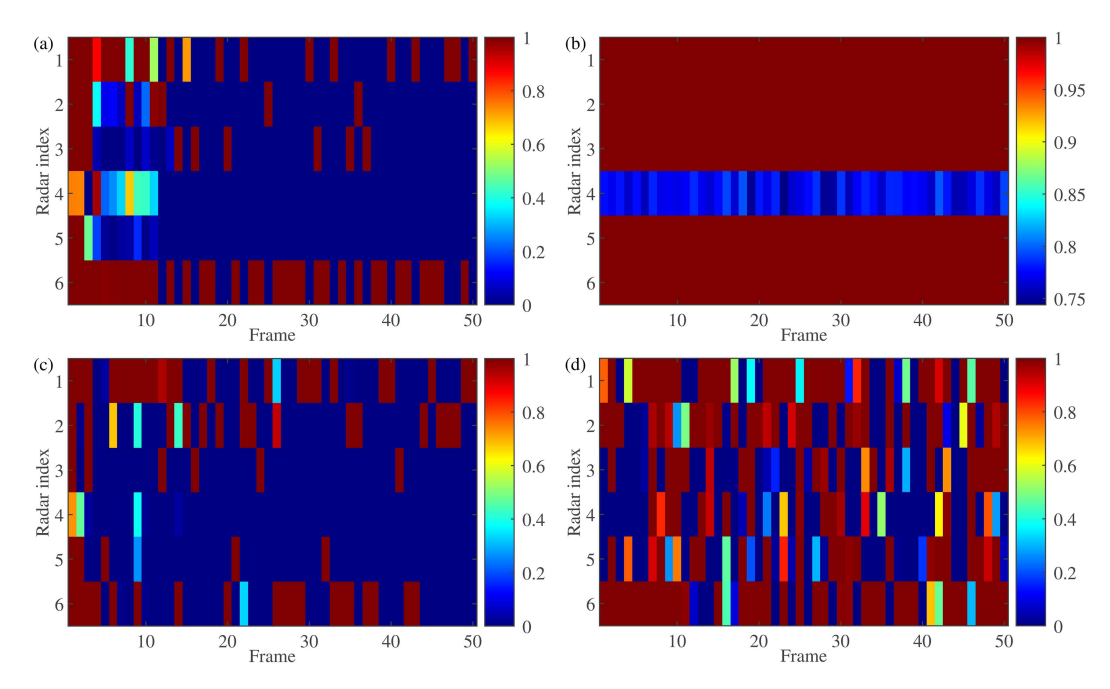
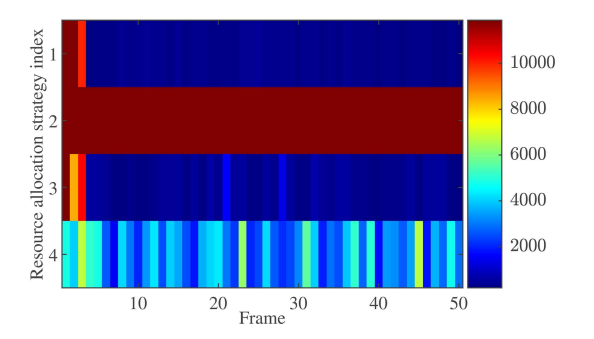


Figure 9 Sorting probability of each radar for four resource allocation strategies. (a) CM; (b) MTEM; (c) MIPM; (d) RM.



loss-free after detection loss after overlap loss

10²
2 20 40

Figure 10 Pulse traffic length for four resource allocation strategies. Note that strategies 1, 2, 3, and 4 refer to CM, MTEM, MIPM, and RM, respectively.

Figure 11 Variation of the number of pulses at frames 2, 20, and 40.

respectively. It can be observed that due to the significant loss of pulses (either undetected or lost due to overlap), the PRI spectra for our strategy and the MIPM exhibit smaller values of pulse counts compared with the other two schemes, and only one PRI can be estimated. In other words, only one radar is detected or intercepted, while the MTEM can intercept all 6 radars and RM can intercept 3 or 4 radars.

To quantitatively compare the anti-interception performance of those resource allocation schemes, 1000 Monte Carlo tests are conducted. The probabilities of sorting each radar are plotted separately in Figure 9. It can be seen that under MTEM, each radar has a high sorting probability throughout the whole process. In contrast, under our strategy and MTEM, the sorting probability most of the time is very low except for the beginning period; for example, under our strategy, radars 4 and 5 realize the whole process of stealth after 12-th frame, whereas under MTEM, radars 3, 4, and 5 can be regarded as almost the entire process of stealth. Under RM, the sorting probability of each radar has both high and low undulation, and there is no regularity to be found, but the overall is still higher than that under our strategy and MTEM.

The LPI performance of the four strategies can be measured by the number of pulses intercepted by the intercept receiver. When the number of pulse sources is determined, the longer the intercepted pulse, the greater the likelihood of finding a radar radiation pattern like PRI. It can be seen from Figure 10 that MTEM radiates a large number of pulses throughout the whole track process. In contrast, the strategy in this paper and MIPM emit a large number of pulses only at the beginning of the tracking and drastically reduce the number of pulses at the later stages. Figure 11 then shows how the strategy proposed in this paper controls the length of the pulse traffic. At the

beginning of the tracking, the number of pulses and the radiated power are significant, and relatively few pulses are lost due to detection, while relatively many pulses are lost due to overlap; at the later stage, the number of emitted pulses itself is minimal, and there is no need to further increase the pulse loss through radiation power and duty cycle control.

In conclusion, the resource allocation scheme proposed in this paper endows the radar network system with low interception performance. Comprehensively comparing these four resource allocation strategies, although the proposed strategy is not optimal in a single comparison of the tracking accuracy and interception resistance metrics, it can take both metrics into account and thus has a wider range of applications.

7 Conclusion

Radar faces the risk of interception by reconnaissance devices while detecting targets. From the perspective of active countermeasures, the paper designed a multi-radar resource allocation scheme in a multi-target tracking scenario to reduce the probability of interception. By building and analyzing the signal model of multi-radar collaborative tracking of multiple targets, the study discovered that radar-controllable variables such as radiation power, dwell time, duty cycle, and radar beam allocation scheme simultaneously affected both the radar's tracking accuracy of targets and the reconnaissance device's interception probability of the radar. By optimizing these variables, a balance between detection performance and stealth performance was achieved. In contrast to existing RF stealth methods that only considered single pulse detection problems, the paper took into account pulse deinterleaving, which was more closely related to the detection of radiation sources. Thus, it fully exploited the potential of the radar network in countering interception.

In analyzing low interception probability, this paper only performed pulse sorting based on PRI information on the received pulse traffic. In reality, electronic interception devices first conduct clustering preprocessing based on relatively stable inter-pulse characteristic parameters, such as arrival angle and carrier frequency before pulse deinterleaving, to achieve sparsity of the pulse traffic. Subsequently, PRI information or other intra-pulse characteristic parameters are utilized for signal selection. As the sorting process in this paper is simplified, further improvement is needed in subsequent research to fit actual scenarios better. In addition, the modeling should be more relevant to the actual situation; for example, radar detection requirements such as the maximum unambiguous distance should also be considered when optimizing the PRI. Optimizing the solution algorithm to fit the real-time tracking process will also be the next research focus.

Acknowledgements This work was supported by National Nature Science Foundation Youth Foundation of China (Grant No. 62301599).

References

- 1 Richards M A, Scheer J A, Holm W A. Principles of Modern Radar: Basic Principles. Raleigh: Scitech, 2010
- 2 Johnston S. Radar electronic counter-countermeasures. IEEE Trans Aerosp Electron Syst, 1978, 14: 109–117
- Li N, Zhang Y. A survey of radar ECM and ECCM. IEEE Trans Aerosp Electron Syst, 1995, 31: 1110–1120
- 4 Neri F. Introduction to Electronic Defense Systems. 3rd ed. Norwood: Artech, 2018
- 5 Farina A. Single sidelobe canceller: theory and evaluation. IEEE Trans Aerospace Electron Syst, 1977, 13: 690-699
- 6 Maisel L. Performance of sidelobe blanking systems. IEEE Trans Aerospace Electron Syst, 1968, 4: 174–180
- 7 Yang X, Zhang Z, Zeng T, et al. Mainlobe interference suppression based on eigen-projection processing and covariance matrix reconstruction. Antennas Wirel Propag Lett, 2014, 13: 1369–1372
- 8 Liu Y, Yu L, Wei Y. Multiple mainlobe jamming suppression via eigen-projection processing blind source separation algorithm. In: Proceedings of IEEE International Radar Conference, Sydney, 2023. 1–6
- 9 Wiley R. ELINT: The Interception and Analysis of Radar Signals. Norwood: Artech, 2006
- 10 Schleher D C. LPI radar: fact or fiction. IEEE Aerosp Electron Syst Mag, 2006, 21: 3–6
- 11 Schleher D C. Low probability of intercept radar. In: Proceedings of IEEE Radar Conference, Washington, 1985. 346-349
- 12 Wu P H. On sensitivity analysis of low probability of intercept (LPI) capability. In: Proceedings of IEEE Military Communications Conference, Atlantic City, 2005. 2889–2895
- 13 Self A G, Smith B G. Intercept time and its prediction. IEE Proc F Commun Radar Signal Process UK, 1985, 132: 215
- 14 Xu L, Zhang T, Ma Z, et al. Power allocation for radar tracking with LPI constraint and suppressive jamming threat. IEEE Trans Aerosp Electron Syst, 2024, 60: 1194–1207
- 15 Lawrence D E. Low probability of intercept antenna array beamforming. IEEE Trans Antennas Propagat, 2010, 58: 2858-2865
- 16 Zhao J, Qiao S, Booske J H, et al. Low probability of intercept/detect (LPI/LPD) secure communications using antenna arrays employing rapid sidelobe time modulation. IEEE Trans Antenna Propagat, 2024, 72: 6448–6463
- 17 Xiong J, Wang W, Cui C, et al. Cognitive FDA-MIMO radar for LPI transmit beamforming. IET Radar Sonar & Navi, 2017, 11: 1574–1580
- 18 Gong P, Zhang Z, Cheng X, et al. Joint design of the transmit and receive beamforming via ADMM for LPI radar. In: Proceedings of IET International Radar Conference (IRC 2023), Chongqing, 2023. 181–185
- 19 Wang X, Yi W, Kong L. Joint beam selection and dwell time allocation for multi-target tracking in phased array radar system. J Radars, 2017, 6: 602–610
- 20 Liu X, Yuan Y, Zhang T, et al. Integrated transmit waveform and RIS phase shift design for LPI detection and communication. IEEE Trans Wireless Commun, 2024, 23: 5663–5679
- 21 Feng X, Wu L, Zhao Y, et al. Recurrent waveform optimization for desired range-Doppler profile with low probability of interception: a particle filter approach. IEEE Trans Aerosp Electron Syst, 2024, 60: 1899–1911
- 22 Chernyak V S. Fundamentals of Multisite Radar Systems: Multistatic Radars and Multiradar Systems. London: Gordon and Breach, 1998
- 23 Geng Z. Evolution of netted radar systems. IEEE Access, 2020, 8: 124961

- 24 Yan J, Jiao H, Pu W, et al. Radar sensor network resource allocation for fused target tracking: a brief review. Inf Fusion, 2022, 86–87: 104–115
- 25 Yan J, Pu W, Zhou S, et al. Collaborative detection and power allocation framework for target tracking in multiple radar system. Inf Fusion, 2020, 55: 173–183
- 26 Krishnamurthy V. Emission management for low probability intercept sensors in network centric warfare. IEEE Trans Aerosp Electron Syst, 2005, 41: 133–152
- 27 Shan G, Xu G, Qiao C. A non-myopic scheduling method of radar sensors for maneuvering target tracking and radiation control. Defence Tech, 2020, 16: 242–250
- 28 Zhang Z, Shan G. Non-myopic sensor scheduling to track multiple reactive targets. IET Signal Process, 2015, 9: 37–47
- 29 Pang C, Shan G. Sensor scheduling based on risk for target tracking. IEEE Sens J, 2019, 19: 8224–8232
- 30 Zhang Z, Shan G. UTS-based foresight optimization of sensor scheduling for low interception risk tracking. Adaptive Control Signal, 2014, 28: 921-931
- 31 Xu G, Pang C, Duan X, et al. Multi-sensor optimization scheduling for target tracking based on PCRLB and a novel intercept probability factor. Electronics, 2019, 8: 140
- 32 Zhang Y, Shan G, Ponomaryov V. A risk-based multisensor optimization scheduling method for target threat assessment. Math Problems Eng, 2019, 2019: 2043727
- 33 Amiriara H, Andargoli S M H, Meghdadi V. Efficient radar-target assignment in low probability of intercept radar networks: a machine-learning approach. IEEE Open J Commun Soc, 2023, 4: 2165–2175
- 34 Shi C, Zhou J, Wang F. Adaptive resource management algorithm for target tracking in radar network based on low probability of intercept. Multidim Syst Sign Process, 2018, 29: 1203-1226
- 35 Shi C, Salous S, Wang F, et al. Power allocation for target detection in radar networks based on low probability of intercept: a cooperative game theoretical strategy. Radio Sci, 2017, 52: 1030–1045
- 36 Lu X, Xu Z, Ren H, et al. LPI-based resource allocation strategy for target tracking in the moving airborne radar network. In: Proceedings of IEEE Radar Conference (RadarConf22), New York City, 2022. 1–6
- 37 Shi C, Wang Y, Salous S, et al. Joint transmit resource management and waveform selection strategy for target tracking in distributed phased array radar network. IEEE Trans Aerosp Electron Syst, 2022, 58: 2762–2778
- 38 Shi C, Dai X, Wang Y, et al. Joint route optimization and multidimensional resource management scheme for airborne radar network in target tracking application. IEEE Syst J, 2022, 16: 6669–6680
- 39 Cui H, Xie L, Ren W, et al. Joint node selection and power allocation in phased array radar network with LPI property and spectral compatibility for multitarget tracking. IEEE Sens J, 2024, 24: 27699-27711
- 40 Shi C, Tang Z, Ding L, et al. Multidomain resource allocation for asynchronous target tracking in heterogeneous multiple radar networks with nonideal detection. IEEE Trans Aerosp Electron Syst, 2024, 60: 2016–2033
- 41 Tichavsky P, Muravchik C H, Nehorai A. Posterior Cramér-Rao bounds for discrete-time nonlinear filtering. IEEE Trans Signal Process, 1998, 46: 1386–1396
- 42 Ljung L. Asymptotic behavior of the extended Kalman filter as a parameter estimator for linear systems. IEEE Trans Automat Contr, 1979, 24: 36–50
- 43 Xie M, Yi W, Kong L, et al. Receive-beam resource allocation for multiple target tracking with distributed MIMO radars. IEEE Trans Aerosp Electron Syst, 2018, 54: 2421–2436
- 44 Djuric P M, Kotecha J H, Zhang J, et al. Particle filtering. IEEE Signal Process Mag, 2003, 20: 19–38
- 45 Liu W, Liu J, Liu T, et al. Detector design and performance analysis for target detection in subspace interference. IEEE Signal Process Lett, 2023, 30: 618–622
- 46 Liu W J, Liu J, Hao C P, et al. Multichannel adaptive signal detection: basic theory and literature review. Sci China Inf Sci, 2022, 65: 121301
- 47 Shortle J F, Thompson J M, Gross D, et al. Fundamentals of Queueing Theory. 5th ed. Hoboken: Wiley, 2017
- 48 Nishiguchi K, Kobayashi M. Improved algorithm for estimating pulse repetition intervals. IEEE Trans Aerosp Electron Syst, 2000, 36: 407–421

Appendix A Derivation of $A_{k,n}^q$, $B_{k,n}^q$, and $C_{k,n}^q$

According to the references¹⁾²⁾, $J_{\rm D}^n(\zeta_{k,n}^q)$ is a 2×2 matrix with each elements calculated as

$$\left[J_{\mathrm{D}}^{n}\left(\boldsymbol{\zeta}_{k,n}^{q}\right)\right]_{ij} = 2\Re\left(\frac{\partial\boldsymbol{\mu}_{k,n}^{q\dagger}}{\partial\left[\boldsymbol{\zeta}_{k,n}^{q}\right]_{i}}\boldsymbol{C}_{n}^{-1}\frac{\partial\boldsymbol{\mu}_{k,n}^{q}}{\partial\left[\boldsymbol{\zeta}_{k,n}^{q}\right]_{j}}\right), i, j = 1, 2,$$
(A1)

where

$$\frac{\partial \boldsymbol{\mu}_{k,n}^{q}}{\partial \left[\boldsymbol{\zeta}_{k,n}^{q}\right]_{i}} = \begin{bmatrix}
\frac{\partial \left[\boldsymbol{\mu}_{k,n}^{q}\right]_{1}}{\partial \left[\boldsymbol{\zeta}_{k,n}^{q}\right]_{i}} \\
\frac{\partial \left[\boldsymbol{\mu}_{k,n}^{q}\right]_{2}}{\partial \left[\boldsymbol{\zeta}_{k,n}^{q}\right]_{i}} \\
\vdots \\
\frac{\partial \left[\boldsymbol{\mu}_{k,n}^{q}\right]_{L_{k,n}M_{\text{t}n}M_{\text{r}n}}}{\partial \left[\boldsymbol{\zeta}_{k,n}^{q}\right]_{i}}
\end{bmatrix}.$$
(A2)

According to (A1), $[J_{\rm D}^n(\zeta_{k,n}^q)]_{11}$ can be calculated as

$$\left[\boldsymbol{J}_{\mathrm{D}}^{n}\left(\boldsymbol{\zeta}_{k,n}^{q}\right)\right]_{11} = \frac{2}{\sigma_{n}^{2}}\Re\left(\frac{\partial\boldsymbol{\mu}_{k,n}^{q\dagger}}{\partial\boldsymbol{\theta}_{k,n}^{q}}\frac{\partial\boldsymbol{\mu}_{k,n}^{q}}{\partial\boldsymbol{\theta}_{k,n}^{q}}\right)$$

¹⁾ Zhang H, Shi J, Zhang Q, et al. Antenna selection for target tracking in collocated MIMO radar. IEEE Trans Aerospace Electron Syst, 2021, 57: 423–436.

²⁾ Kay S M. Fundamentals of Statistical Signal Processing: Estimation Theory. Upper Saddle River: Prentice-Hall, Inc., 1993.

Zhang L, et al. Sci China Inf Sci January 2026, Vol. 69, Iss. 1, 112302:19

$$= \frac{8\pi^{2}\alpha_{k,n}^{q}P_{tk,n}\left|h_{k,n}^{q}\right|^{2}L_{k,n}\cos^{2}\left(\theta_{k,n}^{q}\right)}{\sigma_{n}^{2}\lambda_{n}^{2}M_{tn}} \sum_{m_{tn}=1}^{M_{tn}} \sum_{m_{rn}=1}^{M_{rn}} \left(\left(m_{tn}-1\right)d_{tn}+\left(m_{rn}-1\right)d_{rn}\right)^{2}$$

$$= P_{tk,n}D_{ck,n}T_{dwk,n}A_{k,n}^{q}$$
(A3)

with

$$A_{k,n}^{q} \triangleq \frac{8\pi^{2} \alpha_{k,n}^{q} \left| h_{k,n}^{q} \right|^{2} \cos^{2} \left(\theta_{k,n}^{q} \right)}{\sigma_{n}^{2} \lambda_{n}^{2} M_{\text{tn}} T_{\text{dn}}} \sum_{m_{\text{tn}}=1}^{M_{\text{tn}}} \sum_{m_{\text{tn}}=1}^{M_{\text{rn}}} \left((m_{\text{tn}} - 1) d_{\text{tn}} + (m_{\text{rn}} - 1) d_{\text{rn}} \right)^{2}. \tag{A4}$$

 $\left[\boldsymbol{J}_{\mathrm{D}}^{n}(\boldsymbol{\zeta}_{k,n}^{q}) \right]_{22}$ can be calculated as

$$\left[J_{D}^{n}\left(\zeta_{k,n}^{q}\right)\right]_{22} = \frac{2}{\sigma_{n}^{2}} \Re\left(\frac{\partial \mu_{k,n}^{q\dagger}}{\partial f_{dk,n}^{q}} \frac{\partial \mu_{k,n}^{q}}{\partial f_{dk,n}^{q}}\right) \\
= \frac{8\pi^{2} \alpha_{k,n}^{q} P_{tk,n} \left|h_{k,n}^{q}\right|^{2} M_{rn} T_{rk,n}^{2} L_{k,n} \left(2L_{k,n}-1\right) \left(L_{k,n}-1\right)}{6\sigma_{n}^{2}} \\
\approx \frac{8\pi^{2} \alpha_{k,n}^{q} P_{tk,n} \left|h_{k,n}^{q}\right|^{2} M_{rn} T_{dwk,n}^{3} D_{ck,n}}{3\sigma_{n}^{2} T_{dn}} \\
= P_{tk,n} D_{ck,n} T_{dwk,n}^{3} B_{k,n}^{q} \tag{A5}$$

with

$$B_{k,n}^q \triangleq \frac{8\pi^2 \alpha_{k,n}^q \left| h_{k,n}^q \right|^2 M_{\text{r}n}}{3\sigma_n^2 T_{\text{d}n}}.\tag{A6}$$

 $\left[\pmb{J}_{\rm D}^n(\pmb{\zeta}_{k,n}^q)\right]_{12}$ and $\left[\pmb{J}_{\rm D}^n(\pmb{\zeta}_{k,n}^q)\right]_{21}$ can be calculated as

$$\left[J_{D}^{n}\left(\zeta_{k,n}^{q}\right)\right]_{12} = \frac{2}{\sigma_{n}^{2}}\Re\left(\frac{\partial\mu_{k,n}^{q\dagger}}{\partial\theta_{k,n}^{q}}\frac{\partial\mu_{k,n}^{q}}{\partial f_{dk,n}^{q}}\right) \\
= \frac{8\pi^{2}\alpha_{k,n}^{q}P_{tk,n}\left|h_{k,n}^{q}\right|^{2}\cos\left(\theta_{k,n}^{q}\right)T_{rk,n}L_{k,n}\left(L_{k,n}-1\right)}{2\sigma_{n}^{2}\lambda_{n}M_{tn}}\sum_{m_{tn}=1}^{M_{tn}}\sum_{m_{rn}=1}^{M_{rn}}\left((m_{tn}-1)d_{tn}+(m_{rn}-1)d_{rn}\right) \\
\approx \frac{4\pi^{2}\alpha_{k,n}^{q}P_{tk,n}\left|h_{k,n}^{q}\right|^{2}\cos\left(\theta_{k,n}^{q}\right)T_{dwk,n}^{2}D_{ck,n}}{\sigma_{n}^{2}\lambda_{n}M_{tn}T_{dn}}\sum_{m_{tn}=1}^{M_{tn}}\sum_{m_{rn}=1}^{M_{rn}}\left((m_{tn}-1)d_{tn}+(m_{rn}-1)d_{rn}\right) \\
= P_{tk,n}D_{ck,n}T_{dwk,n}^{2}C_{k,n}^{q} = \left[J_{D}^{n}\left(\zeta_{k,n}^{q}\right)\right]_{21} \tag{A7}$$

with

$$C_{k,n}^{q} \triangleq \frac{4\pi^{2} \alpha_{k,n}^{q} \left| h_{k,n}^{q} \right|^{2} \cos\left(\theta_{k,n}^{q}\right)}{\sigma_{n}^{2} \lambda_{n} M_{\text{tn}} T_{\text{dn}}} \sum_{m_{tn}=1}^{M_{\text{tn}}} \sum_{m_{rn}=1}^{M_{\text{rn}}} \left(\left(m_{\text{tn}} - 1 \right) d_{\text{tn}} + \left(m_{\text{rn}} - 1 \right) d_{\text{rn}} \right). \tag{A8}$$

The aforementioned approximations utilize $L_{k,n} - 1 \approx L_{k,n}$, $2L_{k,n} - 1 \approx 2L_{k,n}$, $T_{\mathrm{dw}k,n} = L_{k,n}T_{\mathrm{r}k,n}$, and $D_{\mathrm{c}k,n} = T_{\mathrm{d}n}/T_{\mathrm{r}k,n}$. Thus, $J_{\mathrm{D}}^{n}(\zeta_{k,n}^{q})$ can be expressed in simplified form like (36).